SACLANTCEN REPORT
serial no: SR-319

SACLANT UNDERSEA RESEARCH CENTRE REPORT

TIMES SERIES VARIABILITY IN FLUCTUATING OCEAN WAVEGUIDES

K.D. LePage

July, 1999

The SACLANT Undersea Research Centre provides the Supreme Allied Commander Atlantic (SACLANT) with scientific and technical assistance under the terms of its NATO charter, which entered into force on 1 February 1963. Without prejudice to this main task — and under the policy direction of SACLANT — the Centre also renders scientific and technical assistance to the individual NATO nations.

SACLANT Undersea Research Centre
Viale San Bartolomeo 400
19138 San Bartolomeo (SP), Italy

tel: +39-0187-5271
fax: +39-0187-524.600

e-mail: library@saclantc.nato.int

NORTH ATLANTIC TREATY ORGANIZATION

Time series variability in fluctuating ocean waveguides

Kevin D. LePage

Executive Summary: Sonar performance is adversly affected by the high degree of variability introduced by internal waves and other oceanographic phenomena in the ocean. In addition, the prediction of acoustic propagation in general is difficult because the environmental information generally available in databases is of poor resolution and is highly uncertain. The result is that actual sonar performance often varies significantly from predictions. For this reason efforts at characterizing the predictability of acoustic propagation through the uncertain ocean are required.

In this report the variability of the temporal arrival structure of a broadband acoustic signal measured in a fluctuating ocean channel is derived. Expressions for the mean and variance of the signal intensity are obtained as functions of the statistical properties of the sound speed uncertainty. The ocean variability is required to be characterized both as a function of depth and of range. These types of characterizations are often available from gridded databases and are also obtainable from CTD casts. The theory uses these characteristics to estimate the resulting statistical properties of the acoustic signals. These statistical properties can then be used to estimate the performance degradation of various sonar systems. As an example, the performance degradation is estimated for one of the advanced sonar concepts being developed here at SACLANTCEN.

intentionally blank page

Time series variability in fluctuating ocean waveguides

Kevin D. LePage

Abstract: The variability of signals propagating through an uncertain sound speed structure is addressed. Signals are assumed to travel in a narrow band adiabatically in modes and to experience fluctuations in sound speed which are characterized according to the vertical and horizontal distributions of these fluctuations. The sound speed fluctuations are assumed to affect only the phase speed and the group speed of the modes in a perturbative way. The changes in the local phase and group speeds are expanded for small perturbations to the sound speed. Sound speed perturbations are described in terms of their statistical characteristics. Vertically, the sound speed fluctuations are decomposed into empirical orthogonal functions (EOFs), while horizontally they are assumed to be correlated on some horizontal length scale much smaller than the propagation ranges of interest. Thus the cumulative phase and group speed fluctuations over the propagation path are assumed to be distributed Gaussian according to the central limit theorem.

The framework outlined above is used to derive the first and second moments of the signal envelope received over an ensemble of ocean realizations following the distribution properties outlined above. Since the mean and variance of the expected signal are obtained in the time domain, the stability of modal arrivals in time can be predicted for a variety of different sound speed fluctuation distributions. Since the phase and group speed fluctuations are linear in identical terms involving the inner product of the mode shape functions with the EOFs, the fluctuations of these quantities are entirely correlated. However, as the different EOFs express themselves differently on each set of propagating modes, the modal interference structure becomes less certain due to the fluctuations. The theory estimates this degree of decorrelation as a function of the signal, waveguide and fluctuation parameters.

In order to benchmark the theory, the first moment of the short time average of the signal intensity is also predicted using realizations of propagation through an ensemble of sound speed fluctuations consistent with the statistical description. Excellent agreement is found between these self-consistent Monte-Carlo estimates of the signal variability and the closed form expressions.

Keywords: signal fluctuations ∘ empirical orthogonal functions (EOF) ∘ complex envelope ∘ narrowband ∘ time reversal mirror ∘ internal waves

Contents

1

Introduction

The fact that acoustic waves travel through significant fine scale and mesoscale sound speed structure between source and receiver at basin and global scales introduces significant variability between time series which might be predicted using only large scale information about the variation in sound channel and actual received time series. As acoustic waves travel through the sound channel, they encounter local variations from the mean sound speed structure predicted by data bases which are introduced by 1) biases between database predictions of sound speed as averages over annual measurements and a particular realization at databases scales (typically 1 degree resolution), and 2) fine scale structure which is inadequately accounted for in the databases, such as internal wave activity. Because of these measurement uncertainties, predicted waveforms which coherently superimpose modes across the band of interest to synthesize a highly coherent snapshot of a particular realization of the sound field will vary significantly from actual measured arrival time series. Since the purpose of predicting time series is to help understand what signals a detector and time of arrival estimator may reliably expect, what is required are estimates of the expected arrival structure averaged over a large number of realizations of sound channel variability.

2
Theory

We propose a simple model for the time series received a great distance from a source which is parameterized not only on deterministic variables such as center frequency, bandwidth, receiver and source depth, but also on uncertainty accumulated along the path introduced by sound channel fluctuations. If we assume that sound channel perturbations introduce local fluctuations in the wavenumber and group speed of modes, and further assume that the fluctuations are not significant enough to cause mode coupling, we arrive at the following expression for the time series received at a receiver in the limit of large range

$$p(t,r,z) \simeq \Re\left\{(2\pi)^{1/2}\sum_{n=1}^{N}\frac{e^{-i(w_o t-\int_0^r k_n^o(r')\,dr'+\int_0^r \triangle k_n(r')\,dr')}}{\sqrt{\int_0^r k_n^o(r')\,dr'}}\phi_n(\omega_o,z_s)\phi_n(\omega_o,z)\right.$$
$$\left.\times\int_{-\triangle\omega}^{\triangle\omega} d\omega e^{-i\omega(t-\int_0^r S_n(r')\,dr'+\int_0^r \triangle S_n(r')\,dr')}\right\}, \quad (1)$$

where $S_n = \frac{\partial k_n}{\partial\omega}$, and $\triangle k_n(r')$, $\triangle S_n(r')$ are the deviations in the modal wavenumbers and slownesses caused by perturbations to the local sound speed structure at range r', and the sub or superscripts o indicate that the quantity has been evaluated at the center frequency. These have been derived before [1, 2] and are reiterated here for convenience

$$\triangle k_n(r') = -\frac{\omega^2}{k_m^o(r')}\int_{-\infty}^{o}\frac{\triangle c(z,r')}{c_o^3(z,r')\rho(z,r')}\phi_n^2(z,r')\,dz. \quad (2)$$

$$\triangle S_n(r') = -\left(2 - S_n(r')\frac{\omega}{k_m^o(r')}\right)\frac{\omega}{k_m^o(r')}\int_{-\infty}^{0}\frac{\triangle c(z,r')}{c_o^3(z,r')\rho(z,r')}\phi_n^2(z,r')\,dz$$
$$-2\frac{\omega^2}{k_m^o(r')}\int_{-\infty}^{o}\frac{\triangle c(z,r')}{c_o^3(z,r')\rho(z,r')}\frac{\partial\phi_n(z,r')}{\partial\omega}\phi_n(z,r')\,dz. \quad (3)$$

It is assumed that all the mean properties of the sound channel at range r' have been characterized in terms of the modal properties k_n, S_n and ϕ_n, and that the remaining uncertainties $\triangle k_n$ and $\triangle S_n$ are well approximated by Eqs. (2) and (3).

2.1 *Characterization of signal variablity in terms of Empirical Orthogonal Functions*

The question of intermodal correlation of the deviations in the wavenumber and slowness to particular realizations in the sound speed perturbations $\triangle c$ leads us to adopt the decomposition of the sound speed fluctuations into Empirical Orthogonal Functions (EOFs,)each of which are by definition uncorrelated for the particular data from which they were obtained, but which, following Krolik [3], will also be assumed to be statistically independent. We seek to understand how the decorrelation between adjacent modes dictates the expected behavior of a received time series. These decorrelations are caused by the differences in the responses of the individual modes to the common sound speed perturbations they encounter as they travel along the propagation path. The use of EOFs allows these differences in response to be decomposed into uncorrelated components; if only one EOF is used then the perturbations between all the modes remain entirely correlated.

The sound speed perturbations are expanded in terms of range dependent coefficients on the EOF bases

$$\triangle c(z,r) = \sum_{e=1}^{E} g_e(r)\psi_e(z),$$

where the bases are estimated from data sets according to the formula

$$\Psi(:,e) = \mathbf{V}(:,e+1)/\sqrt{dz}.$$

Here $\mathbf{V}(:,e+1)$ are the right singular vectors of the singular value decomposition of the sound speed profile covariance

$$\mathbf{U}^{\dagger}\mathbf{S}\mathbf{V} = \sum_{n} \mathbf{c}(r_n)\mathbf{c}^{\dagger}(z,r_n),$$

and $dz = D/N$, where D is the depth of the water column and N is the number of receiver depths.

The first right singular vector $\mathbf{V}(:,1)$ is proportional to the mean or background sound speed profile and thus is not used to describe the random component of the sound speed profile. The range dependent coefficients are determined from the EOF bases according to the relation

$$\mathbf{g}(r) = \left\{\Psi^{\dagger}\Psi\right\}^{-1}\Psi^{\dagger}\mathbf{c}(r). \tag{4}$$

In this way the range integral of the deviations to the modal wavenumber and slowness are determined in terms of known constants and the range integral of the EOF coefficients g

$$\int_0^r \triangle k_n(r')\, dr' = \triangle k_n \sum_{e=1}^{E} \Psi_{en} \overline{g}_e \tag{5}$$

$$\int_0^r \triangle S_n(r')\, dr' = \triangle S_n \sum_{e=1}^{E} \Psi_{en} \overline{g}_e \tag{6}$$

where

$$\triangle k_n = -\frac{\omega^2}{k_m^o(r')},$$

$$\triangle S_n = -\left(2 - S_n(r')\frac{\omega}{k_m^o(r')}\right)\frac{\omega}{k_m^o(r')},$$

$$\Psi_{en} = \int_{-\infty}^{0} \frac{\psi_e(z)}{c_o^3(z,r')\rho(z,r')} \phi_n^2(z,r')\, dz.$$

and

$$\overline{g}_e = \int_0^r g_e(r')\, dr'$$

The range integrals of the EOF coefficients themselves are assumed to be zero mean Gaussian random variables. Thus the range integrals are assumed to cover many correlation lengths of the individual g_e. If the variance of the individual g_e is $\sigma_{g_e}^2$, then the variance of the range integral is

$$\begin{aligned} \sigma_{\overline{g}_e}^2 &= \int_0^r dr' \int_0^r dr'' \langle g_e(r') g_e(r'') \rangle \\ &\simeq \sigma_{g_e}^2 r \ell_e, \end{aligned} \tag{7}$$

where ℓ_e is the correlation scale of the horizontal variability of the EOF coefficient g_e. If this horizontal variability is homogeneous with known power spectrum P_{g_e}, then the variance may be expressed in terms of the spectral integral [4]

$$\sigma_{\overline{g}_e}^2 = r^2 \int_{-\infty}^{\infty} dk P_{g_e}(k) sinc^2(kr/2),$$

where the spectral integral of the power spectrum P with the $sinc^2$ function yields the exact ratio of the correlation length scale to the range ℓ_e/r.

2.2 The Short Time Average of the received intensity

The Short Time Average (STA) [1] of the square of Eq. (1) is given by the expression

$$
\begin{aligned}
p^2_{STA}(t,r,z) \;\simeq\; & 2\pi \sum_{n=1}^{N}\sum_{m=1}^{N} \frac{e^{i\int_0^r k_n^o(r')-k_m^o(r')\,dr'}}{\sqrt{\int_0^r k_n^o(r')\,dr' \int_0^r k_m^o(r')\,dr'}} \phi_n^o(z_s)\phi_m^o(z_s)\phi_n^o(z)\phi_m^o(z) \\
& \times \int_{-\Delta\omega}^{\Delta\omega} d\omega_1 \int_{-\Delta\omega}^{\Delta\omega} d\omega_2 \; e^{-i\omega_1(t-S_n r)} e^{i\omega_2(t-S_m r)} \\
& \times \prod_{e=1}^{E} e^{i(\Delta k_{en}-\Delta k_{em}+\omega_1\Delta S_{en}-\omega_2\Delta S_{em})\overline{g}_e}, \qquad (8)
\end{aligned}
$$

where $\Delta k_{en} = \Delta k_n \Psi_e$, $\Delta S_{en} = \Delta S_n \Psi_e$ and $\Delta\omega$ is the bandwidth of interest.

Assuming the $\overline{g}_e$ are uncorrelated, the expected value of the STA of the signal intensity is

$$
\begin{aligned}
\langle p^2_{STA}(t,r,z)\rangle \;\simeq\; & 2\pi \sum_{n=1}^{N}\sum_{m=1}^{N} \frac{e^{i\int_0^r k_n^o(r')-k_m^o(r')\,dr'}}{\sqrt{\int_0^r k_n^o(r')\,dr' \int_0^r k_m^o(r')\,dr'}} \phi_n^o(z_s)\phi_m^o(z_s)\phi_n^o(z)\phi_m^o(z) \\
& \times \int_{-\Delta\omega}^{\Delta\omega} d\omega_1 \int_{-\Delta\omega}^{\Delta\omega} d\omega_2 \; e^{-i\omega_1(t-S_n r)} e^{i\omega_2(t-S_m r)} \\
& \times \prod_{e=1}^{E} e^{-(\Delta k_{en}-\Delta k_{em}+\omega_1\Delta S_{en}-\omega_2\Delta S_{em})^2\sigma^2_{g_e} r\ell_e/2}. \qquad (9)
\end{aligned}
$$

Note in Eq. (9) that the deviations of the slowness and the horizontal wavenumber are entirely correlated. This is a consequence of the fact that these deviations are both derived under a local approximation and are both the result of linear operations on Δc.

Squaring the argument of the exponent on the third line of Eq. (9) and collecting like terms, we see that the decorrelation between adjacent modes at time t and range r is accounted for through the evaluation of the following two dimensional frequency integration

$$
\begin{aligned}
\rho^2_{nm,r,t}(\omega_o,\Delta\omega) \;=\; & e^{-\Theta^2_{nm}} \int_{-\Delta\omega}^{\Delta\omega} d\omega_1 \; e^{-i\omega_1(t-S_n r)} e^{-\omega_1\Theta_1^2} e^{-\omega_1^2\Theta_{11}^2} \\
& \times \int_{-\Delta\omega}^{\Delta\omega} d\omega_2 \; e^{i\omega_2(t-S_m r)} e^{-\omega_2\Theta_2^2} e^{\omega_1\omega_2\Theta_{12}^2} e^{-\omega_2^2\Theta_{22}^2}, \qquad (10)
\end{aligned}
$$

[1] The short time average is taken over times sufficiently long to cancel out the $2\times$ carrier ripples in the waveform which arise when it is squared. Thus the short time average is taken over time scales proportional to $1/f^o$.

where

$$\begin{aligned}
\Theta_{nm}^2 &= \sum_e (\triangle k_{en}^2 - 2 \triangle k_{en} \triangle k_{em} + \triangle k_{em}^2) \sigma_{g_e}^2 r \ell_e / 2 \\
\Theta_1^2 &= \sum_e (\triangle k_{en} - \triangle k_{em}) \triangle S_{en} \sigma_{g_e}^2 r \ell_e) \\
\Theta_{11}^2 &= \sum_e \triangle S_{en}^2 \sigma_{g_e}^2 r \ell_e / 2 \\
\Theta_2^2 &= \sum_e (\triangle k_{em} - \triangle k_{en}) \triangle S_{em} \sigma_{g_e}^2 r \ell_e \\
\Theta_{12}^2 &= \sum_e \triangle S_{en} \triangle S_{em} \sigma_{g_e}^2 r \ell_e \\
\Theta_{22}^2 &= \sum_e \triangle S_{em}^2 \sigma_{g_e}^2 r \ell_e / 2.
\end{aligned}$$

The intermodal decorrelation term associated with Θ_{nm} is the modal decorrelation at ω_o which has been derived previously [3]. The quadratic decorrelation terms Θ_{11} and Θ_{22} can lead to pulse spreading due to decorrelation of adjacent frequencies; the way to see this is that in the absence of the linear decorrelation terms $\Theta_{1,2}$, when $\Theta_{11,22}$ are on the order of one over the bandwidth, $1/\triangle\omega$, the frequency integrals are asymptotically evaluated as the characteristic function

$$\int_{-\triangle\omega}^{\triangle\omega} d\omega_1 \, e^{-i\omega_1(t-S_n r)} e^{-\omega_1^2 \Theta_{11}^2} = \sqrt{\pi/\Theta_{11}^2} e^{-(t-S_n r)^2/4\Theta_{11}^2}.$$

The frequency integrals in Eq. (10) may be performed in closed form if instead of modeling the signal as absolutely band limited, we adopt the use of a Gaussian amplitude spectrum on the signal of effective width $\triangle\omega$. Then Eq. (10) may be rewritten as

$$\begin{aligned}
\rho_{nm,r,t}^2(\omega_o, \triangle\omega) &= e^{-\Theta_{nm}^2} \int_{-\infty}^{\infty} d\omega_1 \, e^{-\omega_1^2/2\triangle\omega^2} e^{-i\omega_1(t-S_n r)} e^{-\omega_1 \Theta_1^2} e^{-\omega_1^2 \Theta_{11}^2} \\
&\quad \times \int_{-\infty}^{\infty} d\omega_2 \, e^{-\omega_2^2/2\triangle\omega^2} e^{i\omega_2(t-S_m r)} e^{-\omega_2 \Theta_2^2} e^{\omega_1 \omega_2 \Theta_{12}^2} e^{-\omega_2^2 \Theta_{22}^2} \quad (11)
\end{aligned}$$

Eq. (11) may be evaluated in closed form. The resulting expression for the STA of the received intensity is (see Annex A for the details of the derivation,)

$$\begin{aligned}\langle p^2_{STA}(t,r,z)\rangle \;\simeq\; & 2\pi \sum_{n=1}^{N}\sum_{m=1}^{N} \frac{e^{i\int_0^r k_n^o(r')-k_m^o(r')\,dr'}}{\sqrt{\int_0^r k_n^o(r')\,dr' \int_0^r k_m^o(r')\,dr'}} \phi_n^o(z_s)\phi_m^o(z_s)\phi_n^o(z)\phi_m^o(z) \\ & \times\sqrt{\pi/(\Theta_{22}^2 + 1/2\,\triangle\,\omega^2)} \\ & \times\sqrt{\pi/(\Theta_{11}^2 + 1/2\,\triangle\,\omega^2 - \Theta_{12}^4/(4\Theta_{22}^2 + 2/\triangle\,\omega^2))} \\ & \times \exp\left(\frac{\Theta_2^4 - (t-\tau_m(r))^2 - i2\Theta_2^2(t-\tau_m(r))}{4\Theta_{22}^2 + 2/\triangle\,\omega^2}\right) \\ & \times \exp\left(\frac{\left[\Theta_1^2 - \frac{2i\Theta_{12}^2(t-\tau_m(r)) - 2\Theta_2^2\Theta_{12}^2}{4\Theta_{22}^2+2/\triangle\omega^2} + i(t-\tau_n(r))\right]^2}{4\Theta_{11}^2 + 2/\triangle\,\omega^2 - \Theta_{12}^4/(\Theta_{22}^2 + 1/2\,\triangle\,\omega^2)}\right), \end{aligned} \tag{12}$$

where $\tau_{n,m}(r) = \int_0^r S_{n,m}(r')\,dr'$.

Eq. (12) evaluates the expected value of the STA of the received intensity. It is also of interest to evaluate the fluctuations of this STA as a function of sound channel variability. What is desired is

$$\sigma^2_{STA}(t,r,z) \equiv \langle p^4_{STA}(t,r,z)\rangle - \langle p^2_{STA}(t,r,z)\rangle^2$$

which may be written explicitly as

$$\begin{aligned}\sigma^2_{STA} \;\simeq\; & 4\pi^2 \sum_{n=1}^{N}\sum_{m=1}^{N}\sum_{n'=1}^{N}\sum_{m'=1}^{N} \phi_n^o(z_s)\phi_m^o(z_s)\phi_{n'}^o(z_s)\phi_{m'}^o(z_s)\phi_n^o(z)\phi_m^o(z)\phi_{n'}^o(z)\phi_{m'}^o(z) \\ & \times \frac{e^{i\int_0^r (k_n^o(r')+k_{n'}^o(r')) - (k_m^o(r')+k_{m'}^o(r'))\,dr'}}{\sqrt{\int_0^r k_n^o(r')\,dr' \int_0^r k_{n'}^o(r')\,dr' \int_0^r k_m^o(r')\,dr' \int_0^r k_{m'}^o(r')\,dr'}} \\ & \times \int_{-\infty}^{\infty} d\omega_1 \int_{-\infty}^{\infty} d\omega_2\; e^{-\omega_1^2/2\triangle\omega^2} e^{-i\omega_1(t-\tau_n(r))} e^{-\omega_2^2/2\triangle\omega^2} e^{i\omega_2(t-S_m r)} \\ & \times \int_{-\infty}^{\infty} d\omega_{1'} \int_{-\infty}^{\infty} d\omega_{2'}\; e^{-\omega_{1'}^2/2\triangle\omega^2} e^{-i\omega_{1'}(t-\tau_{n'}(r))} e^{-\omega_{2'}^2/2\triangle\omega^2} e^{i\omega_{2'}(t-\tau_{m'}(r))} \\ & \times \prod_{e=1}^{E} \exp\{-(\triangle k_{en} + \triangle k_{en'} - (\triangle k_{em} + \triangle k_{em'}) + \omega_1 \triangle S_{en} + \omega_{1'} \triangle S_{en'} \\ & \qquad -(\omega_2 \triangle S_{em} + \omega_{2'} \triangle S_{em'}))^2 \sigma_{g_e}^2 r\ell_e/2\} \\ & - \langle p^2_{STA}(t,r,z)\rangle^2. \end{aligned} \tag{13}$$

Using the same technique used for the ensemble average, the second moment of the ensemble average may be evaluated in closed form. The result is given in Annex B.

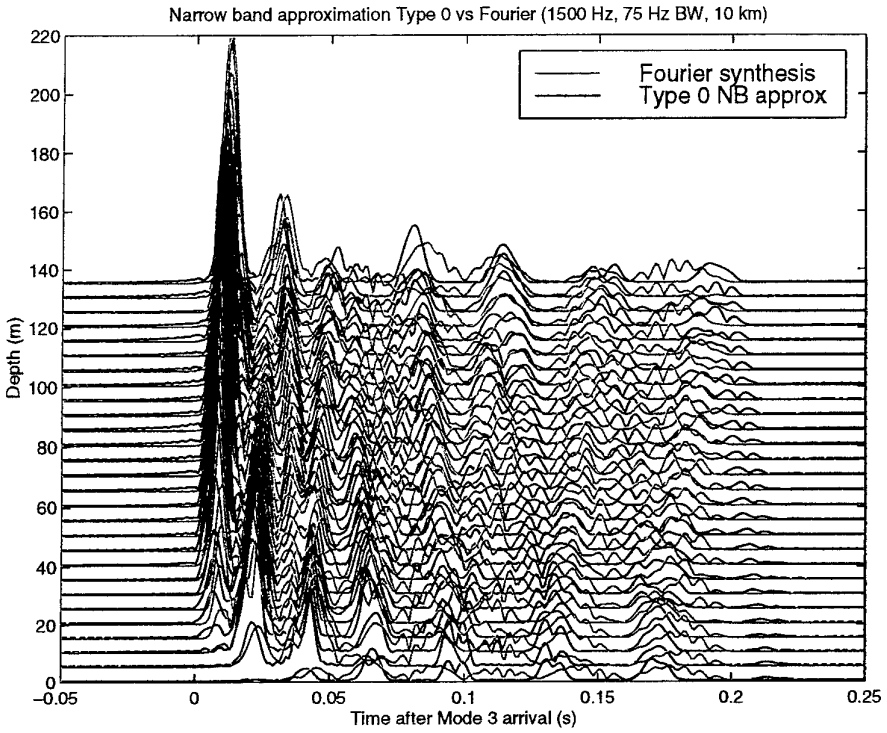

Figure 1 *Comparison between envelope of the Fourier synthesized impulse response and the envelope of the Type 0 narrow band approximation. Agreement in general is poor because the Type 0 narrow band approximation neglects the dispersion of the individual modal arrivals.*

Note that the scintillation index $\imath$ may be obtained from $\sigma^2_{STA}(t,r,z)$ according to the relation

$$\imath \equiv \frac{\sigma^2_{STA}(t,r,z)}{\langle p^2_{STA}(t,r,z)\rangle^2}.$$

This measure is often used to charcaterize signal variability in a random channel.

2.3 Dispersive effects

In the derivations in the previous section it has been assumed that the unperturbed impulse response in the waveguide is well approximated as

$$p(t,r,z) \simeq \Re\left\{(2\pi)^{1/2}\sum_{n=1}^{N}\frac{e^{-i(w_o t-k_n^o r)}}{\sqrt{k_n^o r}}\phi_n(\omega_o,z_s)\phi_n(\omega_o,z) \times \int_{-\infty}^{\infty} d\omega e^{-i\omega(t-S_n r)}e^{-\omega^2/2\Delta\omega^2}\right\}, \quad (14)$$

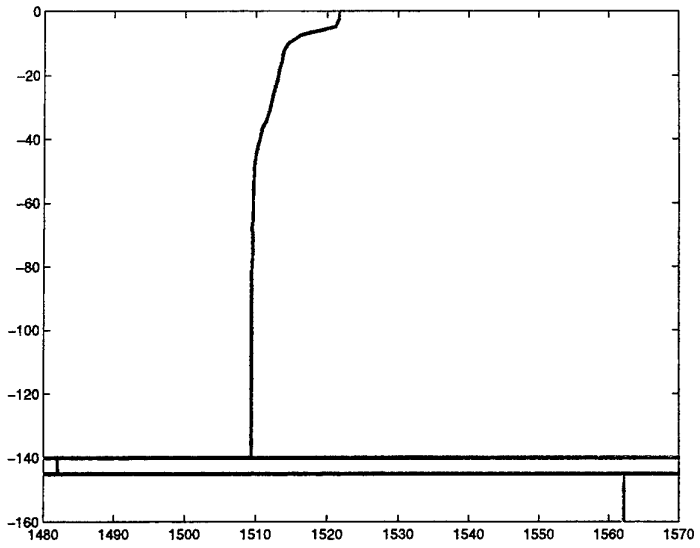

Figure 2 *Shallow water sound speed profile used in this example. The profile is downward refracting and overlies a slow isospeed sediment* 5 *m thick.*

which can be evaluated in closed form as

$$p(t,r,z) \simeq 2\pi \triangle \omega \sum_{n=1}^{N} \frac{\cos(-i(w_o t - k_n^o r))e^{-(t-S_n r)^2 \triangle \omega^2/2}}{\sqrt{k_n^o r}} \phi_n(\omega_o, z_s)\phi_n(\omega_o, z). \quad (15)$$

In reality Eq. (15), which we call the Type 0 narrow band approximation, is highly inaccurate since it neglects the pulse dispersion in the individual modes which is so important for determining the coherent interference pattern as a function of depth and time at reasonable ranges. This can be seen in Figure 1 where the envelope of the Fourier synthesized Green's function at 1500 Hz and 75 Hz of bandwidth for a shallow water waveguide is compared to the envelope of the Type 0 narrow band approximation. The approximation agrees poorly because it simply places each mode at an arrival time determined by the modal slowness S_n, neglecting the spreading of the mode arrivals in time which leads to the ray-like interference effect seen in the Fourier synthesized result.

The sound speed profile for the shallow water environment is shown in Figure 2. Since the slow sediment layer carries the first two modes at 1500 Hz, the travel times in this discussion are referred to the first arriving waterborne mode, Mode 3. The dispersion curves for the waveguide are illustrated in Figure 3, and show typical shallow water behavior. While the phase speed of the first two modes is quite slow due to the slow sediment layer, the phase speeds for modes 3 – 70 increase with increasing mode number, as expected. The group speed of the first two modes is also slow due to the fact that they are trapped in the slow sediment, but as expected

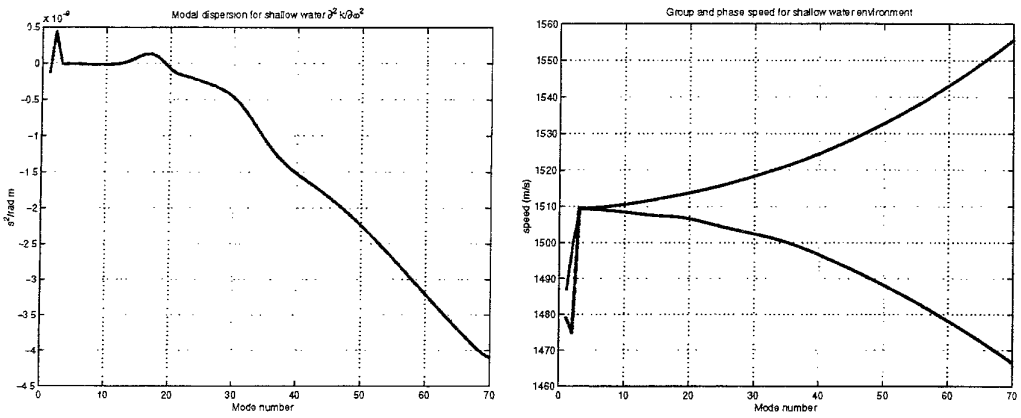

Figure 3 *The dispersion curves for the shallow water waveguide at* 1500 *Hz. The left panel is shows the curvature term* $\partial^2 k/\partial\omega^2$*, while the right panel showns the phase and group speed.* 70 *modes are supported, the first two of which live in the sediment layer.*

the waterborne modes have decreasing group speed for increasing mode number. The modal dispersion term is negative, indicating that at higher frequencies a given mode is less slow than it is at lower frequencies

$$S_n(\omega + \omega_o) = S_n(\omega_o) - |D_n|\,(\omega - \omega_o)/2,$$

which we have also observed to be typical shallow water behavior. For this reason time series in shallow water waveguides arrive in an inverse frequency chirp, with the highest frequencies arriving first.

2.3.1 *Type 1 narrow band approximation*

A better approximation to the waveguide Green's function is obtained when the second order modal dispersion term $D_n \equiv \frac{\partial^2 k_n}{\partial\omega^2}$ is included in the phase argument of the complex exponential

$$\begin{aligned} p(t,r,z) \;\simeq\; & \Re\left\{(2\pi)^{1/2}\sum_{n=1}^{N}\frac{e^{-i(w_o t - k_n^o r)}}{\sqrt{k_n^o r}}\phi_n(\omega_o,z_s)\phi_n(\omega_o,z)\right. \\ & \left.\times\int_{-\infty}^{\infty} d\omega e^{-i\omega(t-(S_n+\omega D_n r/2)}e^{-\omega^2/2\Delta\omega^2}\right\}. \end{aligned} \tag{16}$$

This frequency integral can also be evaluated in closed form to obtain what we call a first order narrow band approximation

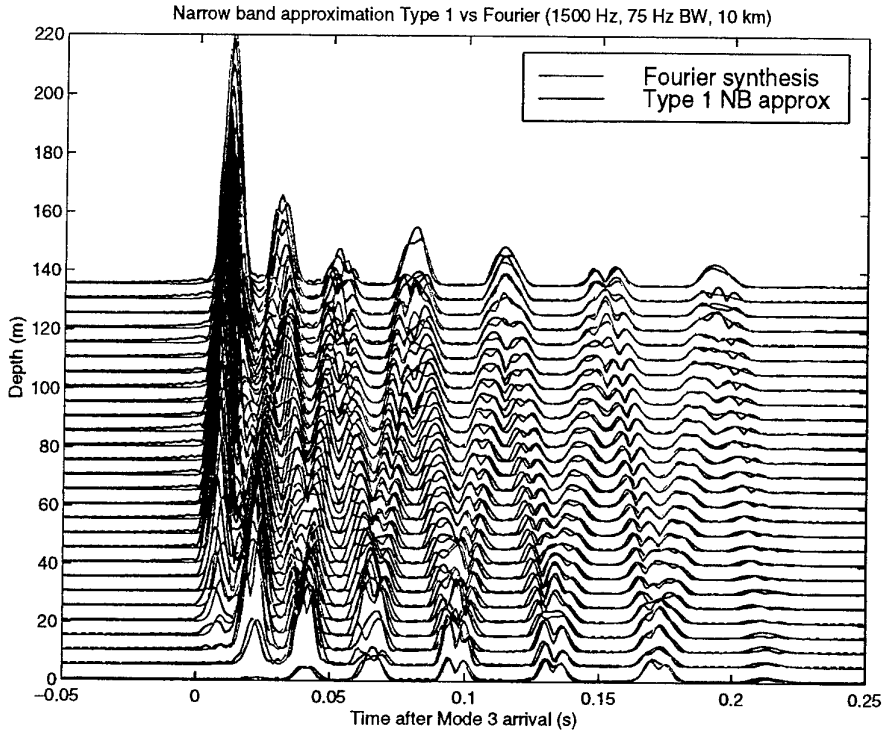

Figure 4 *The performance of the Type 1 narrow band approximation is superior to the Type 0 shown in Figure 1. The effects of modal dispersion are now accurately modeled, leading to better estimates of the modal interference which gives the true coherent propagation structure.*

$$p(t,r,z) \simeq \Re\left\{(2\pi)^{1/2}\sum_{n=1}^{N}\frac{e^{-i(w_o t-k_n^o r)}}{\sqrt{k_n^o r}}\phi_n(\omega_o,z_s)\phi_n(\omega_o,z)\right.$$
$$\left.\times\sqrt{\frac{2\pi}{\triangle\omega^{-2}-iD_n r}}\exp\left\{-\frac{(t-S_n r)^2}{2(\triangle\omega^{-2}-iD_n r)}\right\}\right\}. \qquad (17)$$

As shown in Figure 4, the first order narrow band approximation for the waveguide Green's function does a better job of replicating the coherent arrival structure of the Fourier synthesized result.

The importance of modal dispersion implies that a modal arrival time is an abstraction which in practice does not exist. Instead, the modes disperse sufficiently such that they always overlap their neighbors in time. This means there is a fundamental lack of resolution of the modal arrival time which is introduced by the waveguide and which in general bandwidth will not remove. The modal dispersion which allows the strong interference between modes spreads the arrival time of an individual

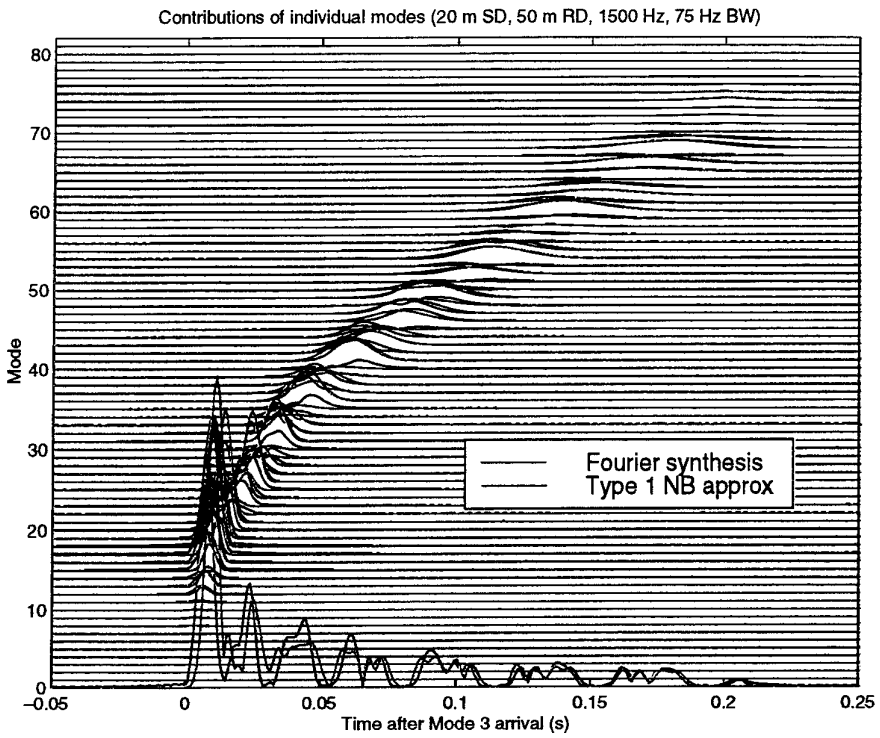

Figure 5 *The envelopes of the individual modal contributions to the total response received at a depth of* 50 *m. This figure showns that the estimation of modal arrival times is not meaningful at this frequency and range. Individual mode envelopes are highly overlapped due to dispersion of the individual modes. The Type 1 narrow band approximation shown in red does a fairly good job of predicting the response, but under or over estimates individual model arrivals due to the assumption that the mode shapes are independent of frequency.*

mode out over times large with respect to the time scales of total summed response. This effect is illustrated in Figure 5, where the envelopes of the individual modal arrivals for a receiver at a depth of 50 m in the water column are shown for all the propagating modes, along with the envelope of the coherent sum which is related to what would be measured in an experiment. The black curves are the exact Fourier synthesized results, which extend up to 82 modes over the entire frequency band of the synthesis, while the red curves are the the Type 1 narrow band approximation, which is obtained by assuming that the 70 modes present at the center frequency exist over the entire frequency band of interest (instead there are 68 modes at 1425 Hz and 75 at 1575 Hz.)

From the results shown in Figure 5 it is clear that an experimentally measured quantity such as the arrival time of a large pulse in the total time series has no

2.3.2 Type 2 narrow band approximation

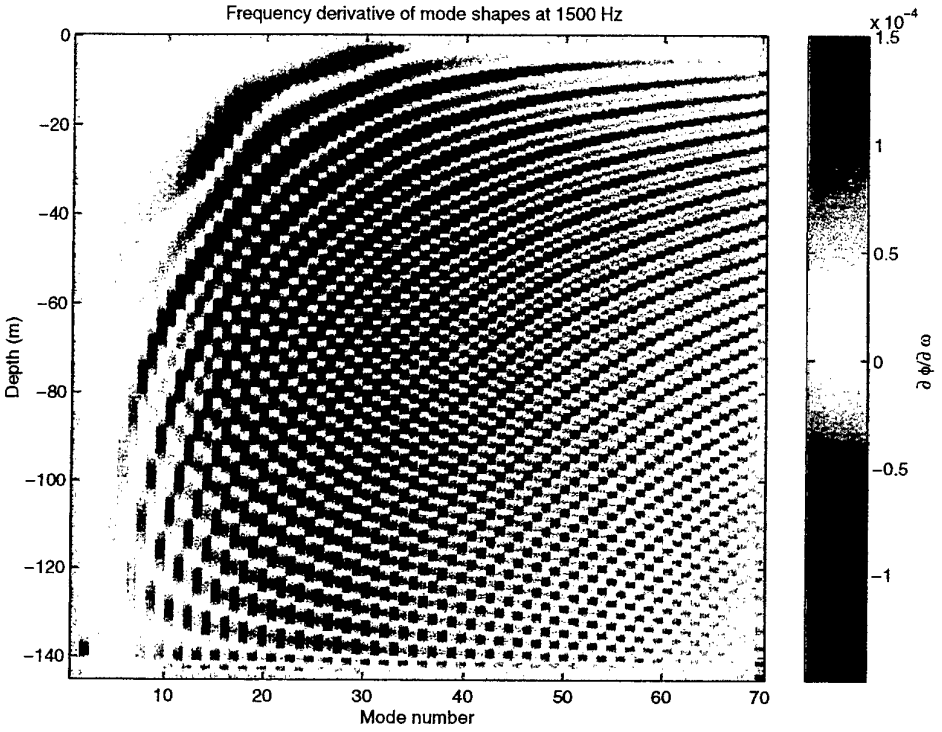

Figure 7 *The frequency derivative of the shallow water mode shapes at* 1500 *Hz. The mode shapes are rather strong functions of frequency.*

The fact that the mode shapes can be strong functions of frequency even in relatively narrow frequency bands compared to the center frequency of interest implies that a first order Taylor series correction to the modes shapes of the form

$$(2\pi)^{1/2} \sum_{n=1}^{N} \frac{e^{-i(w_o t - k_n^o r)}}{\sqrt{k_n^o r}} \left\{ \phi_n(\omega_o, z_s) \left. \frac{\partial \phi_n(z)}{\partial \omega} \right|_{\omega_o} + \phi_n(\omega_o, z) \left. \frac{\partial \phi_n(z_s)}{\partial \omega} \right|_{\omega_o} \right\}$$
$$\times \int_{-\infty}^{\infty} d\omega \; \omega \; e^{-i\omega(t-(S_n+\omega D_n r/2)} e^{-\omega^2/2\triangle\omega^2} \quad , \qquad (18)$$

can be added inside the brackets of Eq. (16) to obtain improved performance.

The numerical values of $\partial\phi/\partial\omega$ as determined by finite differences for our example waveguide are illustrated as a function of depth and mode number in Figure 7. Using these values Eq. (18) can be evaluated to obtain the complex representation of the correction which when placed in the brackets of Eq. (17) leads to a second order or

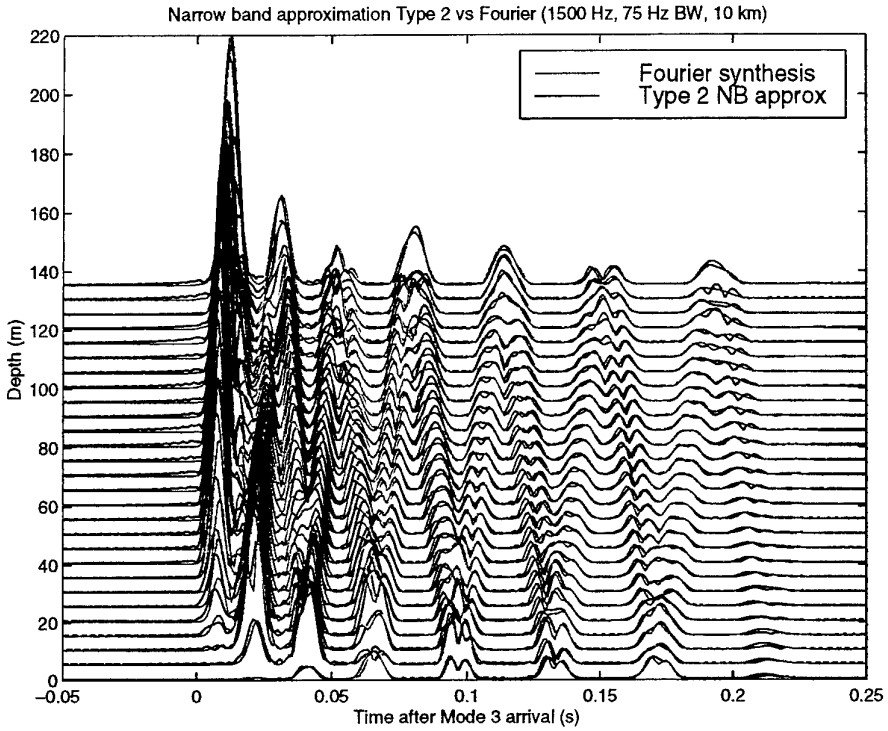

Figure 8 *The Type 2 narrow band approximation bears a strong resemblance to the true channel impulse response. For this reason the theory of time series stability developed in this report is based on the Type 2 narrow band approximation.*

Type 2 narrow band approximation

$$
\begin{aligned}
p(t,r,z) \;\simeq\; & (2\pi)^{1/2}\Re\left\{\sum_{n=1}^{N}\frac{e^{-i(w_o t-k_n^o r)}}{\sqrt{k_n^o r}}\sqrt{\frac{2\pi}{\triangle\omega^{-2}-iD_n r}}\exp\left\{-\frac{(t-S_n r)^2}{2(\triangle\omega^{-2}-iD_n r)}\right\}\right. \\
\times\; & \left\{\phi_n(\omega_o,z_s)\left(\phi_n(\omega_o,z)+\left(\frac{i(S_n r-t)}{2(\triangle\omega^{-2}-iD_n r)}\right)\left.\frac{\partial\phi_n(z)}{\partial\omega}\right|_{\omega_o}\right)\right. \\
& \left.\left.+\;\phi_n(\omega_o,z)\left(\phi_n(\omega_o,z_s)+\left(\frac{i(S_n r-t)}{2(\triangle\omega^{-2}-iD_n r)}\right)\left.\frac{\partial\phi_n(z_s)}{\partial\omega}\right|_{\omega_o}\right)\right\}\right\}.
\end{aligned}
\tag{19}
$$

The performance of the Type 2 narrow band approximation is illustrated in Figure 8 superimposed on the Fourier synthesized result. This agreement is considered to be sufficiently good to faithfully model the overall characteristics of the time domain Green's function of a waveguide. In Figure 9 the constituent modal components of the total time series for a receiver depth of 50 m are illustrated for both the Fourier synthesized Green's function and the Type 2 narrow band approximation.

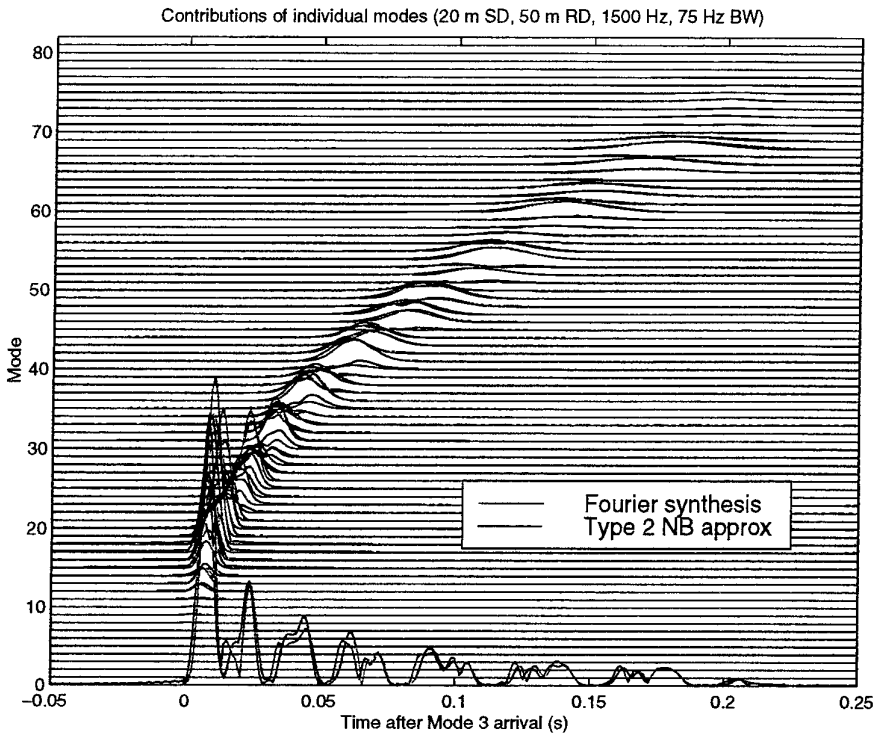

Figure 9 *The performance of the Type 2 narrow band approximation as a function of mode number. These results are significantly better than the Type 1 results in Figure 5.*

Comparison with Figure 5 shows the Type 2 approximation does a better job of modeling the temporal characteristics of the intermediate mode numbers, allowing more accurate modeling of the total response.

2.4 Inclusion of dispersive effects in expressions for p^2_{STA}

The dispersive effects associated with the Type 1 narrow band approximation are introduced into Eq. (12) and Eq. (34) by making the substitution

$$1/2 \triangle \omega^2 \rightarrow 1/2 \triangle \omega^2 - iD_n r/2.$$

This substitution neglects the effect of terms of the form $\triangle D_n$, which are assumed to be negligible. This approximation is generally found to be valid, as will be shown in the results section. The modification to Eq. (12) to conform to the Type 2 narrow band approximation is more complicated and is therefore presented in detail in Annex C.

2.5 Time Reversal Mirror performance

The theory described in this section to model waveform stability can be used as the basis for a study on the performance of a Time Reversal Mirror (TRM) [5, 6, 7]. A TRM receives a source pulse on a VLA, reverses it in time and rebroadcasts it. At and near the spatial location of the original source a substantial degree of focusing is found to occur. If we assume that the TRM time series are measured for an unperturbed waveguide, we can study the effect of the random sound speed fluctuations on the focus performance. Under the Type 1 narrow band approximation, the time series measured at a depth z and range r from a source at zero range and a depth z_s is

$$\begin{aligned} p(t,z,r|z_s) &\simeq \sum_n \frac{\phi_n(z_s)\phi_n(z)}{\sqrt{k_n r}} \int d\omega\, e^{-i\omega t + \left(k + (\omega-w_o)S_n + (\omega-\omega_o)^2/2D_n\right)r} e^{-(\omega-\omega_o)^2/2\Delta\omega^2} \\ &\simeq \sum_n \frac{\phi_n(z_s)\phi_n(z)}{\sqrt{k_n r}} e^{-i(\omega t - k_o r)} \int d\omega\, e^{-i\omega(t-S_n r)} e^{-\omega^2\left(1/2\Delta\omega^2 - iD_n r/2\right)}. \quad (20) \end{aligned}$$

In a TRM, the received time series is reversed and re-broadcast at the receiver depths. A non-causal time reversal operation is equivalent to a conjugation operation in the frequency domain

$$p(-t) \equiv F^{-1}\left\{\tilde{p}^*(\omega)\right\}.$$

Assuming that the re-broadcast time series is scaled by a factor of $r/\rho(z)$ to remove the effects of cylindrical spreading to and from the source position and to enable the invocation of modal orthogonality in subsequent steps, the complex spectrum of the TRM sources is

$$\tilde{p}^*(\omega,z) = \sqrt{r}\sum_n \frac{\phi_n(z_s)\phi_n(z)}{\sqrt{k_n}\rho(z)} e^{-ik_n r} e^{-i\omega S_n r} e^{-\omega^2\left(1/2\Delta\omega^2 + iD_n r/2\right)},$$

so that the complex spectrum received through a perturbed waveguide in the vicinity of the source range and depth is

$$\begin{aligned} \tilde{p}(\omega,\Delta z,\Delta r) = \sum_N \sum_n \sum_m & \frac{\phi_n(z_s)\phi_m(z_s+\Delta z)\phi_n(z_N)\phi_m(z_N)}{\sqrt{k_m^* k_n}\rho(z_N)} \\ & \times e^{i\omega((S_m+\Delta S_m)(r+\Delta r))} e^{-i\omega S_n r} e^{i((k_m+\Delta k_m)(r+\Delta r))} e^{-ik_n^* r} \\ & \times e^{-\omega^2(-iD_m(r+\Delta r)/2)} e^{-\omega^2\left(1/2\Delta\omega^2 + iD_n r/2\right)}. \quad (21) \end{aligned}$$

In Eq. (21) the quantities Δk_m and ΔS_m indicate that sound speed perturbations have been introduced into the waveguide since the measurement of the impulse response $p(t,z,r|z_s)$. It is assumed that the dispersion D_m is unaffected by these sound speed perturbations. Since we are interested in evaluating the TRM refocusing performance in the presence of water column variability rather that performance as a function of the number and distribution of the TRM sources, we make the assumption that the TRM sources are fully depth sampling (even into the bottom

for bottom penetrating modes included in the Type 1 narrow band approximation,) so that the orthogonality of the modes may be exploited. We also assume that the mode shapes are not strong enough functions of the water column variability for the orthogonality relation to be seriously degraded. Under these assumptions the sum over N becomes an integral which when evaluated eliminates off-diagonal terms and results in the received spectrum

$$\begin{aligned}\tilde{p}(\omega, \triangle z, \triangle r) &= \sum_n \frac{\phi_n(z_s)\phi_n(z_s+\triangle z)}{|k_n|} e^{ik_n \triangle r} e^{i\triangle k_n (r+\triangle r)} e^{i\omega S_n \triangle r} e^{i\omega \triangle S_n (r+\triangle r)} \\ &\quad \times e^{-2\Im\{k_n\}r} e^{-\Im\{k_n\}\triangle r} e^{-\omega^2/2\triangle\omega^2} e^{i\omega^2 D_n \triangle r/2}. \end{aligned} \tag{22}$$

Discarding the unimportant terms $e^{-\Im\{k_n\}\triangle r}$ and $e^{i\omega^2 D_n \triangle r/2}$, the inverse Fourier transform of Eq. (22) yields the complex time series as a function of time and defocused range $\triangle r$ and depth $\triangle z$ from the original source range and depth

$$\begin{aligned}p(t, \triangle z, \triangle r) &= e^{-i\omega_o t} \sum_n \frac{\phi_n(z_s)\phi_n(z_s+\triangle z)}{|k_n|} e^{ik_n \triangle r} e^{i\triangle k_n (r+\triangle r)} e^{-2\Im\{k_n\}r} \\ &\quad \times \int d\omega_1 e^{-i\omega_1 (t - S_n \triangle r - \triangle S_n (r+\triangle r))} e^{-\omega_1^2/2\triangle\omega^2}. \end{aligned} \tag{23}$$

Since the TRM defined here is non-causal, t is the defocusing time about zero time, when the ideal TRM concentrates its energy in depth and range about the original source position.

The expected value of the STA of the square of Eq. (23) is analogous to Eq. (9)

$$\begin{aligned}\langle p^2_{TRM}(t, \triangle r, \triangle z)\rangle &\simeq 2\pi \sum_{n=1}^{N}\sum_{m=1}^{N} \frac{e^{i(k_n - k_m)\triangle r} e^{-2(\Im\{k_n\}+\Im\{k_m\})r}}{|k_n|\,|k_m|} \phi_n(z_s)\phi_m(z_s) \\ &\quad \times \phi_n(z_s+\triangle z)\phi_m(z_s+\triangle z) \int_{-\triangle\omega}^{\triangle\omega} d\omega_1 \int_{-\triangle\omega}^{\triangle\omega} d\omega_2\, e^{-i\omega_1 (t - S_n \triangle r)} e^{i\omega_2 (t - S_m \triangle r)} \\ &\quad \times \prod_{e=1}^{E} e^{-(\triangle k_{en} - \triangle k_{em} + \omega_1 \triangle S_{en} - \omega_2 \triangle S_{em})^2 \sigma^2_{g_e} r \ell_e / 2} e^{-\omega_1^2/2\triangle\omega^2} e^{-\omega_2^2/2\triangle\omega^2} \end{aligned} \tag{24}$$

so that a result equivalent to Eq. (12) is easily determined as

$$\begin{aligned}\langle p^2_{TRM}(t, \triangle r, \triangle z)\rangle &\simeq 2\pi \sum_{n=1}^{N}\sum_{m=1}^{N} \frac{e^{i(k_n - k_m)\triangle r}}{|k_n|\,|k_m|} e^{-2(\Im\{k_n\}+\Im\{k_m\})r} \\ &\quad \times \phi^o_n(z_s)\phi^o_m(z_s)\phi^o_n(z_s+\triangle z)\phi^o_m(z_s \triangle z) \sqrt{\pi/(\Theta^2_{22} + 1/2\,\triangle\omega^2)} \\ &\quad \times \sqrt{\pi/(\Theta^2_{11} + 1/2\,\triangle\omega^2 - \Theta^4_{12}/(4\Theta^2_{22} + 2/\triangle\omega^2))} \\ &\quad \times \exp\left(\frac{\Theta^4_2 - (t - S_m \triangle r)^2 - i2\Theta^2_2 (t - S_m \triangle r)}{4\Theta^2_{22} + 2/\triangle\omega^2}\right) \\ &\quad \times \exp\left(\frac{\left[\Theta^2_1 - \frac{2i\Theta^2_{12}(t - S_m\triangle r) - 2\Theta^2_2\Theta^2_{12}}{4\Theta^2_{22}+2/\triangle\omega^2} + i(t - S_n \triangle r)\right]^2}{4\Theta^2_{11} + 2/\triangle\omega^2 - \Theta^4_{12}/(\Theta^2_{22} + 1/2\,\triangle\omega^2)}\right) \end{aligned} \tag{25}$$

3
Results

3.1 Internal wave characteristics in shallow water

Internal wave realizations were computed using the internal wave realization generator in the PROSIM [8] simulation package. The internal wave realization generator was executed using an energy level of 320 m^2cph, a default buoyancy frequency profile as given in Elliot *et. al.* [9], and a typical summer downward refracting shallow water profile as measured north of Formica in the Tyrrhenian sea during the PROSIM '97 experiment [10]. The resulting perturbations of the sound speed from the background profile are illustrated in the left panel of Figure 10. In general the results show that the strongest perturbations are found in the vicinity of the transition region in the sound speed between the iso-velocity warm surface layer and the colder deeper water. The first 9 EOF's obtained from this realization are illustrated in the right panel of the same figure. The EOF mode shapes are in general confined to the upper third of the water column, with the shallowest penetration for the lowest order, and most energetic, modes. The EOF mode shapes shown obey the relation $\int \psi_n^2(z)\, dz \equiv 1$.

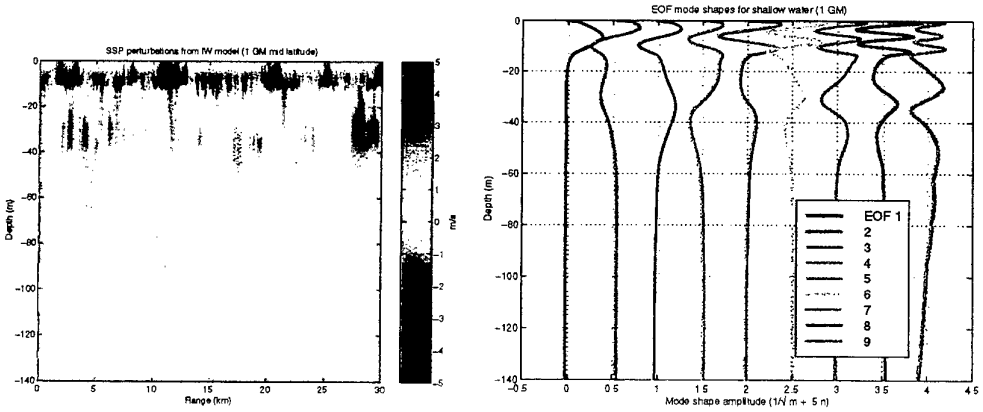

Figure 10 *Internal wave realization and first 9 EOFs for the shallow water environment and a spectrum level of 1 GM.*

The standard deviation of the EOF power expressed in m/s is illustrated in the left panel of Figure 11. The rms amplitude of the first EOF is approximately 0.6 m/s,

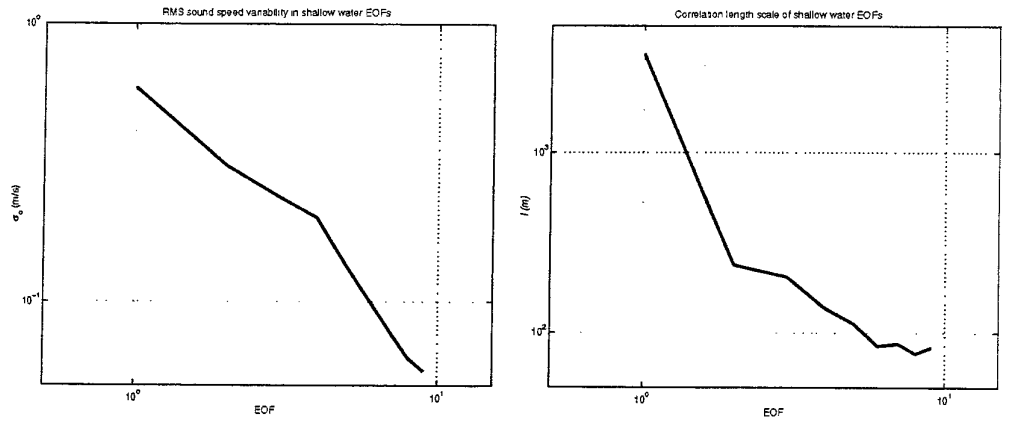

Figure 11 *RMS amplitude and correlation length scale of the shallow water EOFs.*

while for the 9th EOF it is about one order of magnitude smaller. The rms excursion of an EOF as a function of depth is obtained by multiplying the rms amplitude of the mode function (units m/s) together with the mode shape (units $1/\sqrt{\mathrm{m}}$) scaled by the square root of the total water column depth D in meters. Thus the maximum rms excursion of the first EOF is approximately 2.5 m/s, while for the 9th EOF it is only 0.13 m/s. The correlation length scale ℓ of the EOFs is indicated in the right panel of Figure 11. These results indicate that the correlation length scale of the EOFs decreases with increasing mode number, with $\ell_1 \simeq 3500$ m for the first EOF and only $\ell_9 \simeq 80$ m for the 9th. The correlation length scale was estimated by fitting a power law spectrum of the form

$$P_{g_e}(k) \propto (1 + k^2 \ell_e^2)^{-\nu}$$

to the spatial spectrum of the range dependent EOF coefficients

$$P_{g_e}(k) \simeq \left\| \int dx \; g_e(r) e^{ikr} \right\|^2 ,$$

where the range dependent coefficients $\mathbf{g}$ are determined according to Eq. (4). An example of the quality of one of these fits is given in Figure 12.

3.2 Waveform stability in shallow water

Using the EOF properties obtained from the internal wave realization in the previous section, the stability of the arrival time envelope for the range independent shallow water waveguide whos properties are illustrated in Figures 2 and 3 has been computed using Eq. (12). The results are illustrated in Figure 13. The top panel shows the magnitude of the complex envelope of the unperturbed waveguide response for

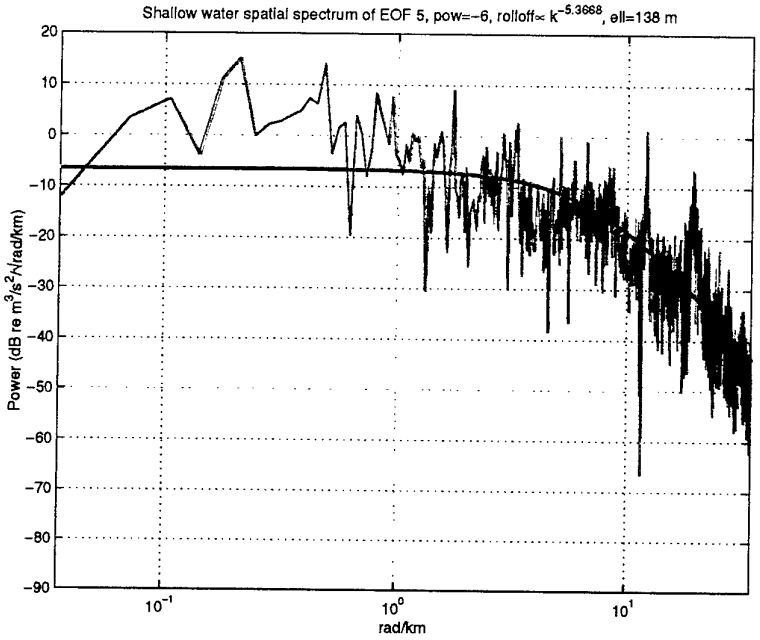

Figure 12 *The Direct Method power spectral estimate of the range dependent EOF coefficient of ψ_5 and the power law fit for the correlation length scale, determined in this case to be* 138 *m.*

the Type 2 narrow band approximation. The second panel illustrates the ensemble average of the STA of the intensity as estimated over 50 realizations of perturbed sound speed profiles using a modified form of Eq. (19),

$$
\begin{aligned}
p(t,r,z) \;\simeq\; & (2\pi)^{1/2}\Re\left\{\sum_{n=1}^{N}\frac{e^{-i(w_o t-k_n^p r)}}{\sqrt{k_n^o r}}\sqrt{\frac{2\pi}{\triangle\omega^{-2}+iD_n^p r}}\exp\left\{-\frac{(t-S_n^p r)^2}{2(\triangle\omega^{-2}+iD_n^p r)}\right\}\right. \\
\times\; & \left\{\phi_n(\omega_o,z_s)\left(\phi_n(\omega_o,z)+\left(\frac{i(S_n^p r-t)}{2(\triangle\omega^{-2}+iD_n^p r)}\right)\left.\frac{\partial\phi_n(z)}{\partial\omega}\right|_{\omega_o}\right)\right. \\
& \left.\left.+\;\phi_n(\omega_o,z)\left(\phi_n(\omega_o,z_s)+\left(\frac{i(S_n^p r-t)}{2(\triangle\omega^{-2}+iD_n^p r)}\right)\left.\frac{\partial\phi_n(z_s)}{\partial\omega}\right|_{\omega_o}\right)\right\}\right\},
\end{aligned}
\tag{26}
$$

where

$$
k_n^p = k_n^o + \triangle k_n \sum_{e=1}^{E} \Psi_{en}\overline{g}_e,
$$

$$
S_n^p = S_n + \triangle S_n \sum_{e=1}^{E} \Psi_{en}\overline{g}_e,
$$

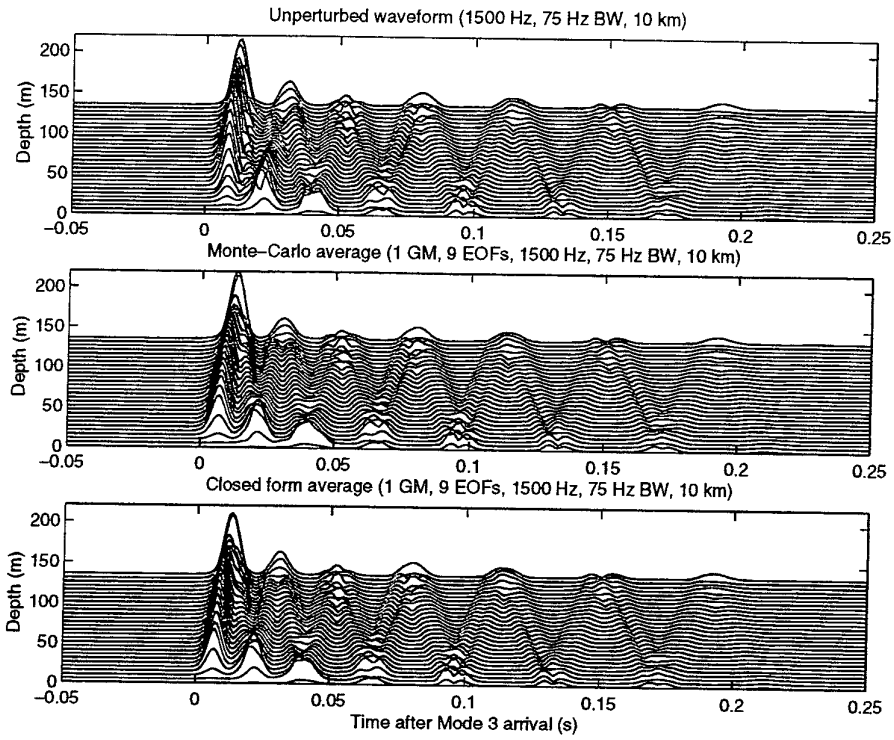

Figure 13 *The unperturbed (top), Monte-Carlo (middle) and closed form (bottom) time-depth arrival structure for a VLA 10 km away from a source in the shallow water waveguide. The uncertainty introduced by the sound speed fluctuations causes a decrease in the ensemble average of the intensity, shown at early time in the lower two panels, as compared to the unperturbed result in the top panel. The agreement between the Monte-Carlo and the closed form result indicates that the closed form theory captures the variability without requiring Fourier synthesis or Monte-Carlo averaging.*

and

$$D_n^p = D_n + \triangle D_n \sum_{e=1}^{E} \Psi_{en} \overline{g}_e.$$

The lowest panel is the closed form prediction given by Eq. (12). The excellent agreement between the Monte-Carlo result and the closed form result indicates that the omission of terms caused by $\triangle D_n$ in the closed form result have not seriously affected its accuracy (these terms were included in the Monte-Carlo result.) The expected value of the STA of the received intensity estimated by either means assumes the absence of mode coupling and the adiabaticity of the sound propagation through the sound speed perturbations.

The results in Figure 13 indicate that the sound speed perturbations caused by

internal wave activity have the strongest influence on the lowest order modes which contribute to the beginning of the time series. This is confirmed by Figure 14, which illustrates the contribution of the SSP perturbation EOFs to the various mode numbers for unity EOF variance $\sigma^2_{g_e}$. The results show that the phase uncertainty $\triangle k_{en}$ introduced by the EOFs most strongly affects modes $3 - 40$, with low EOF indicies introducing more uncertainty than higher ones. The slowness uncertainty $\triangle S_{en}$ and the dispersion uncertainty D_{en} are confined between modes 15 and 45, with the higher EOF indicies contributing more to the uncertainty. The fact that the lower order modes are strongly affected by the EOFs indicates that the earlier part of the time series is less predictable, as the lower two panels in Figure 13 show. Conversely, since modal indicies between 45 and 70 are relatively unaffected by any of the EOFs, the latter part of the time series is shown to be highly predictable.

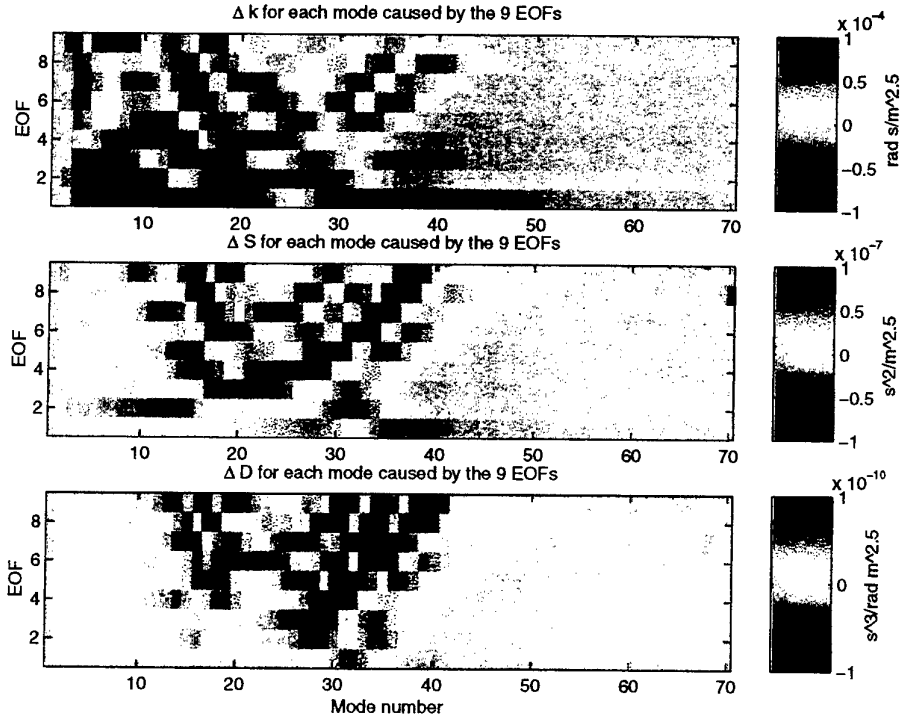

Figure 14 *The perturbations $\triangle k_{em}$ (top), $\triangle S_{em}$ (middle) and $\triangle D_{em}$ (bottom), caused by the 9 EOFs. The variability affects the lower order modes much more strongly than the higher order modes. This explains the fact that the ensemble average of the intensity shows lower levels and more smoothing for the early arriving low order modes, but high predictability for the late arriving modes.*

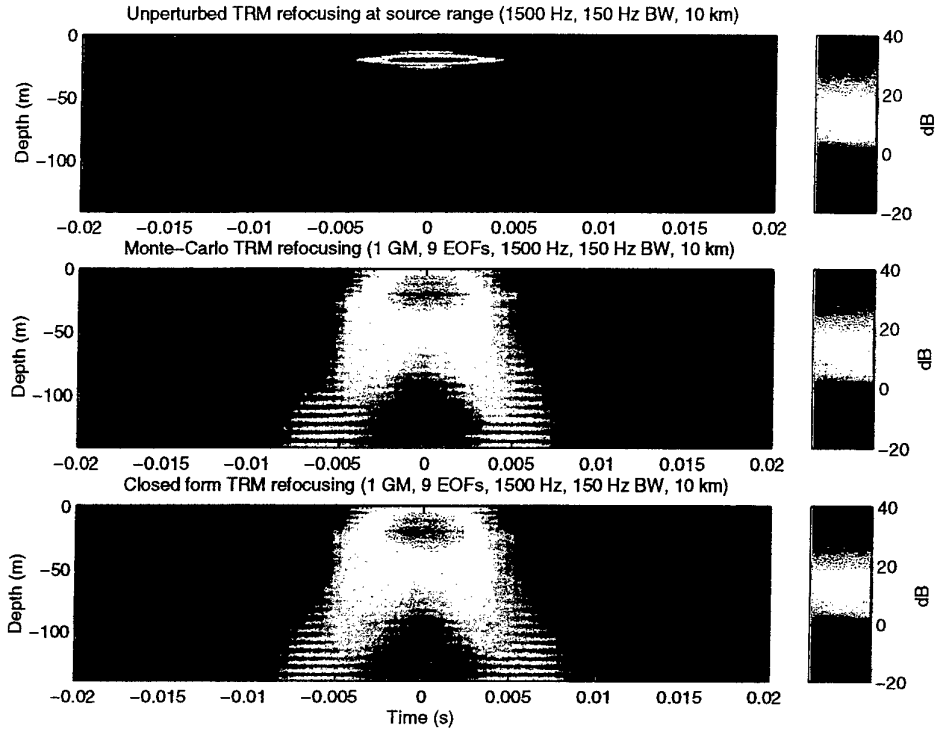

Figure 15 *TRM defocusing in shallow water. The top plot shows the unperturbed focus performance in the time-depth plane, the middle plot the Monte-Carlo average, and the lower plot the closed form solution. Significant defocusing in the ensemble average sense is expected in the case where the sound speed perturbations are present.*

3.3 TRM performance degradation in shallow water

In Figure 15 the performance degradation of the shallow water TRM predicted by Eq. (24) is illustrated in the depth-time plane. The top panel indicates the performance of the ideal TRM, which is well defined in depth with a temporal resolution δt approximately equal to one over the bandwidth (in this case ± 150 Hz rather than the ± 75 Hz used in the previous examples.) The depth resolution is determined by the number of propagating modes and the unrecovered loss of the higher order modes which the TRM cannot eliminate (although a model based TRM which artificially amplifies the higher order modes could recover some of the lost vertical resolution.) In the second panel of Figure 15 the deterioration of the TRM performance is shown in the Monte-Carlo estimate of the TRM depth time response estimated from 50 realizations of environmental perturbations drawn from the distribution parameters derived in the EOF section. A substantial loss in resolution is observed, with significant depth-time spreading along an ambiguous ridge extending from the true source depth down in space-time at an angle determined by the particular physics of the

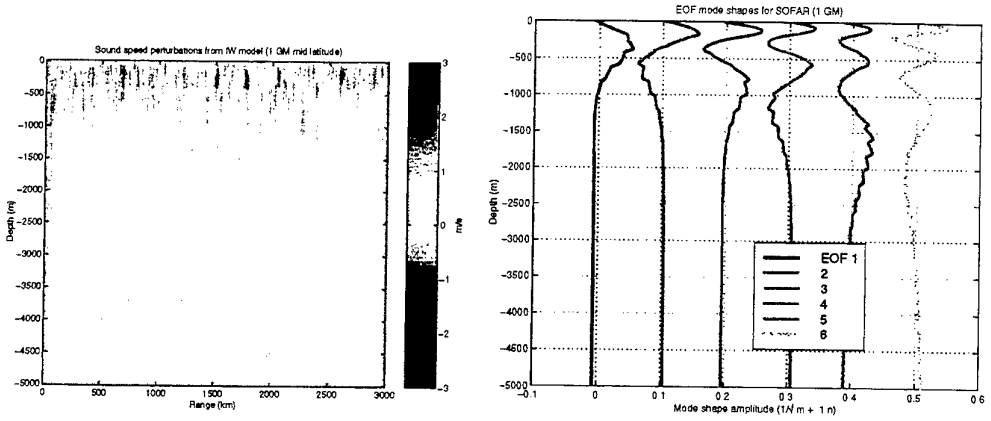

Figure 16 *Internal wave realization for the Munk profile (left) at* 1 *GM. The right plot shows the first 6 EOFs The perturbations and the mode shapes are confined to the water column above the sound speed axis.*

propagation through the perturbed waveguide. The lowest panel shows that the loss in performance is well modeled by the closed form expression in Eq. (24). The results seem to indicate that TRM performance is more strongly affected by waveguide variability than the time series themselves, which were shown in the previous section to be less significantly affected.

3.4 *Internal wave characteristics in a SOFAR channel*

To support the study of waveform predictability in the deep ocean, the PROSIM package was used to generate a 1 GM internal wave realization for a deep water Munk profile [11]. The realization is illustrated in Figure 16 along with the first 6 EOF mode shapes. The EOF mode shapes are confined to the upper 40% of the water column, with the most energetic confined to the upper 20%. The corresponding standard deviation in m/s and correlation length scales are illustrated in Figure 17 The standard deviations, shown in the left panel, are approximately one order of magnitude smaller than in the shallow water case, while the corresponding correlation length scales, shown in the right panel, are $1-2$ orders of magnitude larger, with the largest, for the first EOF, being approximately 100 km. As explained in the theory section, the longer the correlation length scale ℓ_e the more uncertainty is accumulated along a path (assumption always being that path length is longer than correlation length.) However, the uncertainty accumulated is also proportional to the power in the EOFs, which in this case is much lower than it is in shallow water.

The EOF rms sound speed perturbations for the Munk profile drop off much faster than for the shallow water case. For this reason only 6 EOFs were included in the

analysis. Even so there is a drop of almost one order of magnitude between the rms sound speed of the 5th and 6th EOF. The rms sound speed of the 6th EOF is only 0.009 m/s, while the first EOF has an rms sound speed of almost 0.13 m/s. The correlation length scale of the 6th EOF is only 6 km.

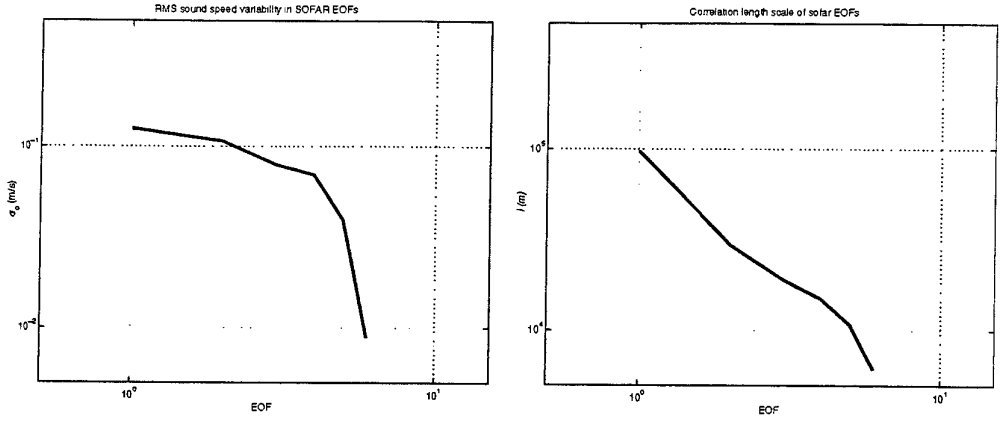

Figure 17 *The RMS amplitude and correlation length scale of the EOFs for the Munk profile. The longest correlation length is* 100 *km.*

The evaluation of the internal wave realization for the Munk profile resulted in sound speed perturbations which were noisier than the shallow water results. This noisyness is not considered to be endemic to the PROSIM model, nor is it considered to be harmful to the validity of the results which are based on this realization. The effect of the noisyness is that the EOFs have higher spatial frequency oscillations superimposed on them which are not considered to be meaningful. While in the subsequent section these oscillations will be shown to introduce some noise into the estimates of the perturbations of the modal dispersion for the 5th and 6th EOF, the contributions of these EOF's to the modal dispersion is so low, and the overall importance of the modal dispersion in general is so negligible, that the results were used in their present form without introducing errors.

3.5 Waveform stability in a SOFAR channel

The Type 2 narrow band approximation was used to estimate the impulse response of the Munk (SOFAR) profile at a receiver range of 1000 km at a center frequency of 100 Hz. The envelope of the resulting time series for 3 Hz of bandwidth is shown along with the envelope of the Fourier synthesized impulse response in Figure 18. The Type 2 narrow band approximation agrees very well for late times, when the axial mode arrivals form the SOFAR crescendo. At earlier times the agreement quantitatively is less good, as the narrow band approximation fails to accurately model the wavefront curvature of the arrival time series near the turning point

depth. However, as before, the agreement is considered to be good enough that the major characteristics of the SOFAR channel impulse response have been captured by the narrow band approximation.

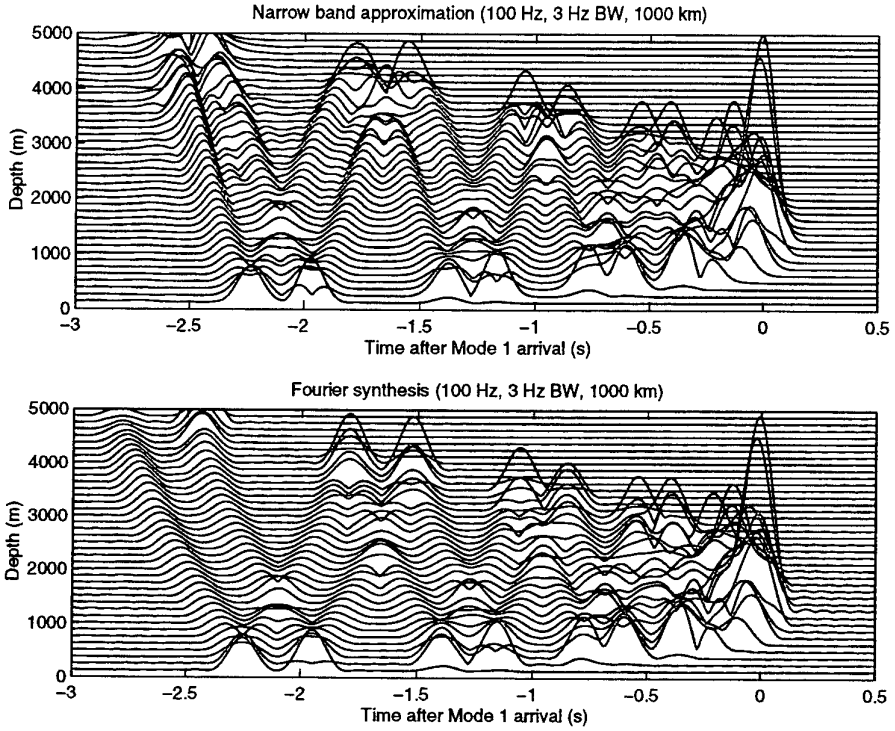

Figure 18 *Performance of the Type 2 narrow band approximation for the SOFAR channel at* 100 *Hz and* 3 *Hz of bandwidth. The agreement is good qualitatively at early times, and quantitatively at late times in the proximity of the SOFAR crescendo.*

The time-depth response of the SOFAR channel is in most ways the opposite of the shallow water channel. Inspection of the group speeds and modal dispersion in Figure 19 show why. In the SOFAR channel, the group speed of the higher order modes is faster than the group speed of the first mode, rather than slower as in the shallow water waveguide. In addition, the modal dispersion is positive rather than negative. The result is that in the SOFAR waveguide the higher frequencies are slower than the lower frequencies, so that the SOFAR crescendo is an up-chirp. The overall result is that the impulse response of the SOFAR channel is characterized by the early arrival of high-angle precursors, with a final crescendo on the SOFAR axis associated with the lowest order modes.

Using the internal wave EOF mode shapes, correlation length scales and power obtained in the previous section, the ensemble average of the STA of the received intensity in a SOFAR channel was predicted by a Monte-Carlo average over 50 re-

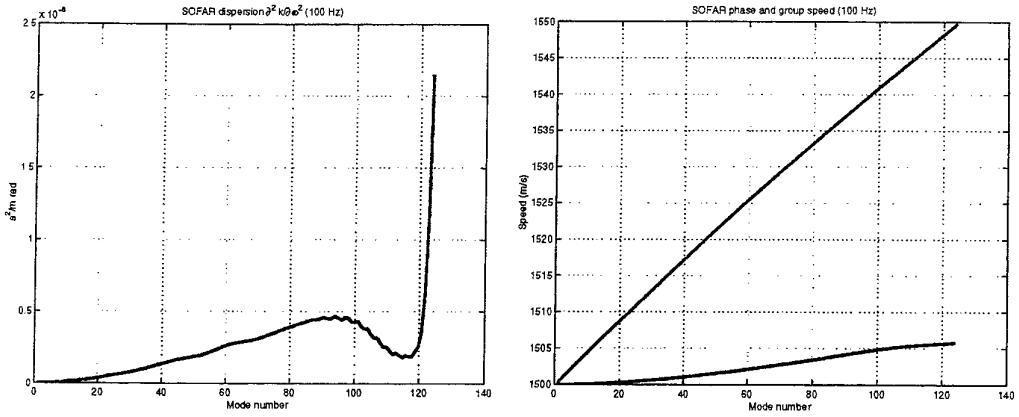

Figure 19 *The modal dispersion $\partial^2 k/\partial\omega^2$ (left) and the phase (red) and group speed (blue) of the SOFAR channel. Positive modal dispersion implies that arrivals are up-chirps (arrive low frequencies first.)*

alizations and through the evaluation of Eq. (12). The result is shown in Figure 20. The upper panel is the unperturbed impulse response from the Type 2 narrow band approximation, the middle panel is the Monte-Carlo average while the lowest panel is the closed form result. The results show that like the shallow water case, it is the lowest order modes which have the most uncertainty, reflected in lower levels for the ensemble averaged STA of intensity versus the unperturbed levels at late times on the SOFAR axis. Thus the theory predicts uncertainty in the crescendo, but relative stability of the high angle precursors. Inspection of the modal perturbations to the wavenumbers, slownesses and modal dispersion in Figure 21 show the reason why. As in shallow water, the modal phase, shown in the upper panel, is most strongly perturbed by the EOFs in the lower order modes. The slowness perturbations and the modal dispersion perturbations are more strongly felt by the higher order modes, but the overall level of these perturbations is apparently insufficient to cause noticeable spreading in time-depth of the early arrivals [2]. On the other hand, the phase perturbation is evidently sufficiently strong that the predictability of the crescendo structure, when many of the lower order modes arrive at virtually the same time, is negatively affected. This is due to the fact that the presence at one time of many modes makes the coherent sum sensitive to the phase fluctuations introduced by the waveguide variability. Since the fluctuations are in detail unpredictable, the ensemble average has less structure and lower peak values than the unperturbed result.

[2]The noise in the estimates of $\triangle D_{en}$ perturbation for $e = 5, 6$, which were determined by running ORCA for the Munk profile with and without an EOF mode shape perturbation, is not considered real. However, comparison between the Monte-Carlo result, which includes this term, and the closed form result, which ignores it, showns that $\triangle D_{en}$ in general are inconsequential. For this reason the results and conclusions of this section are not affected by these noisy estimates

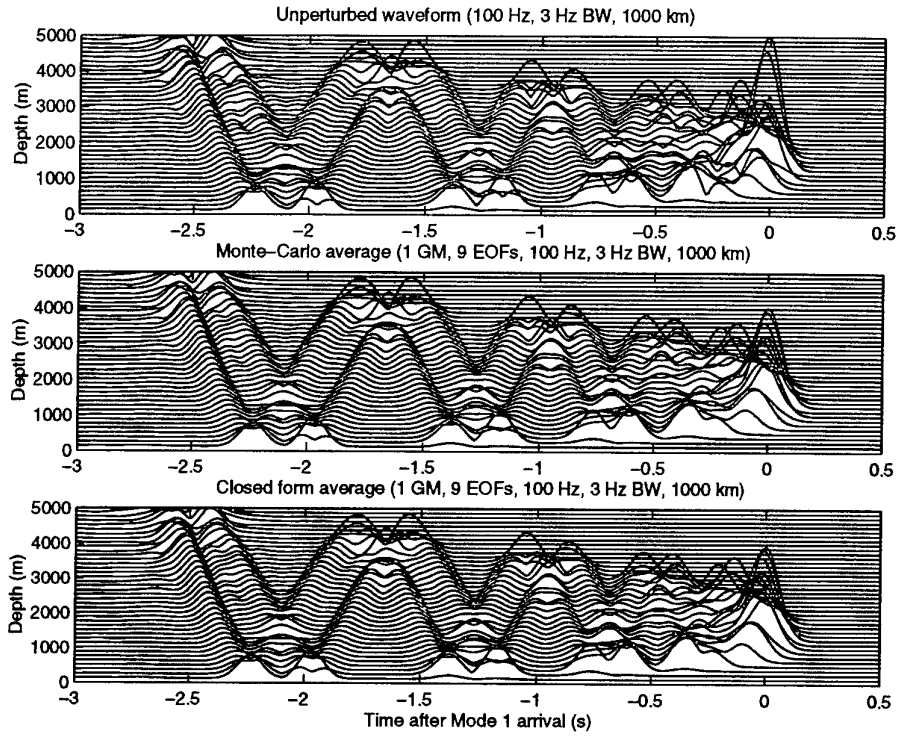

Figure 20 *The unperturbed (top), Monte-Carlo ensemble average of the perturbed (middle) and closed form ensemble average of the perturbed SOFAR channel with 1 GM internal wave fluctuations. The fluctuations affect the predictability of the SOFAR crescendo, reducing the expected value of the intensity since the individual modal arrivals which constitute the crescendo are unpredictable with respect to one another. The high angle precursors are highly predictable as their propagation phase is less strongly affected.*

While the results shown in Figure 20 for the predictability of a SOFAR crescendo are interesting, they do not reflect the true degree of variability which is known to exist in long range time series in the real ocean. The spatial, temporal and angular characteristics of long-range deep water transmissions have been the subject of significant study in recent years [12, 13]. In general it has been shown that mode coupling effects, which are ignored in the theory presented here, are important for explaining most of the variability in time series observed from field experiments. Thus predictions for the variability of the time-depth envelope of long-range SOFAR channel transmissions obtained with the present theory cannot predict several important features commonly observed in experiments, such as the presence at late time of significant energy in higher order modes, and the overall levels of the variability observed for a fixed value of 1 GM in an internal wave field using a Munk sound speed profile. However, some of the other features observed in the data, such as the

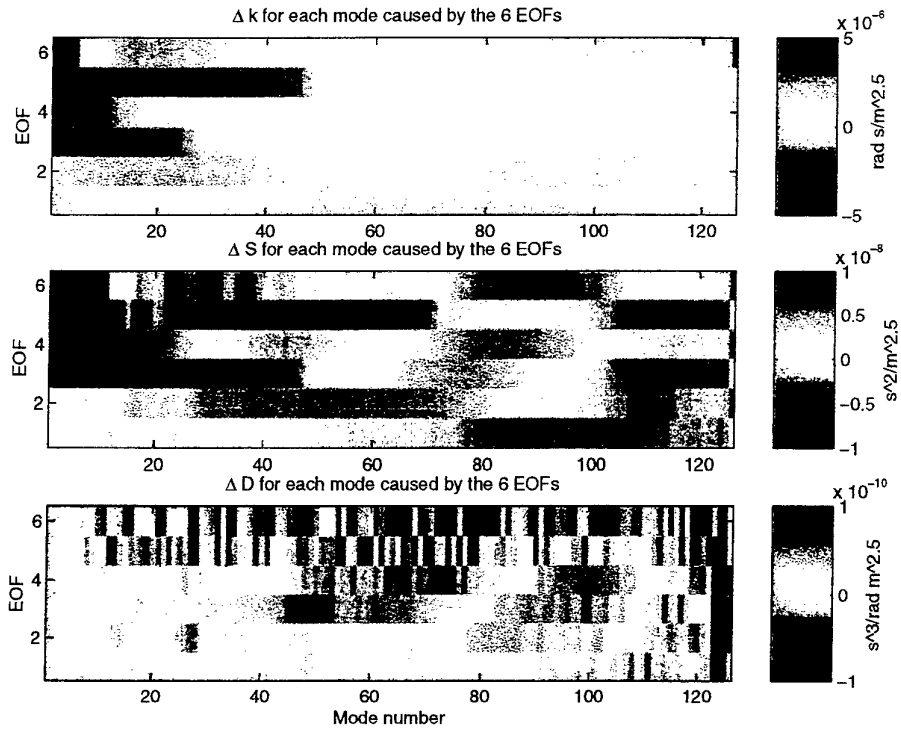

Figure 21 *The perturbations to the phase $\triangle k_{en}$ (top), slowness $\triangle S_{en}$ (middle) and dispersion $\triangle D_{en}$ (bottom) caused by the internal wave sound speed perturbation EOFs in the SOFAR channel. The phase uncertainty is only present for the lower order modes. While the higher order modes suffer some slowness uncertainty, their phase are sufficiently insensitive to the sound speed fluctuations so that their coherent sum remains highly predictable. The noise in the perturbations to the various modes caused by the 5th and 6th EOFS is wrong but does not effect the results, as explained in the text.*

relative stability of the precursor arrivals, and the relatively unpredictable nature of the final crescendo, are predicted by the theory. Thus we view the contribution of the theory presented here to be the theoretical corroboration of the relative stability of the early arrivals under essentially a perturbation analysis. However, the levels of the waveform predictability estimated here are too high, and do not account for the observations of late arrivals of higher order modal energy, which only a coupled mode treatment would predict.

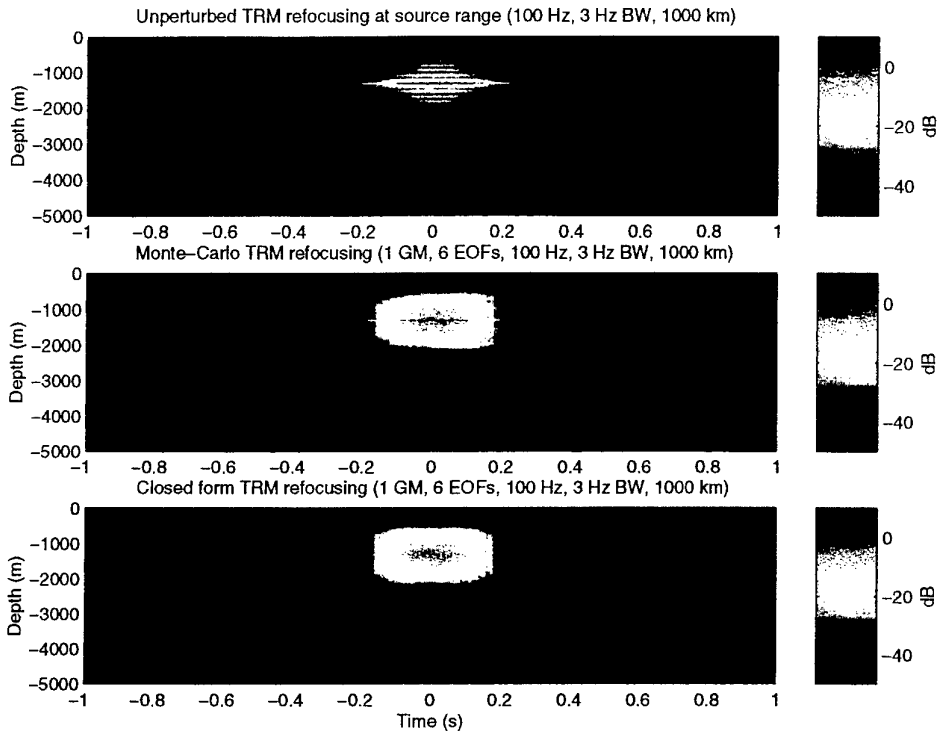

Figure 22 *TRM performance in an unperturbed SOFAR channel (top), and the ensemble average of the focus in the time-depth plane obtained by Monte-Carlo average (middle), and as obtained by the the closed form expression (bottom). Performance is more robust than in the shallow water case, but the environmental perturbations can still be expected to open up the depth focus from a region less than* 100 *m wide to one almost* 1500 *m wide.*

3.6 TRM performance degradation in a SOFAR channel

The degradation of TRM focusing at the 1000 km range is illustrated in Figure 22. The top panel shows the refocusing performance of the unperturbed TRM in the depth-time plane. As in the shallow water case, the resolution of the temporal focus is dictated by the transmitted bandwidth (here 3 Hz), while the depth resolution is controlled by the number of propagating modes and their loss. In the ORCA runs which yielded the complex wavenumbers for this study, only the last 20 modes suffered any propagation loss at all, due to interaction with a lossy bottom, and only modes higher than 121 suffered losses of more than 1 dB. Attenuation due to relaxation processes in the water column were ignored. Thus the depth resolution is quite good in the unperturbed case. The ensemble averaged results of the intensity both for Monte-Carlo (middle panel) and closed form (bottom panel) show very little decrease in the temporal performance of the refocusing, but there is a sub-

stantial decrease in the depth performance. The focus region is significantly blurred across the sound channel axis between the depths of 500 and 2000 meters, while the unperturbed focus region is confined to depths between 1250 and 1350 m. Both the Monte-Carlo average and the closed form solution agree on the amount and the spatial characteristics of the blurring introduced by the water column variability.

4
Conclusions

A comprehensive theory to describe the stability of time series received in waveguides has been developed. The approach is unique in that closed form expressions for perturbed and unperturbed impulse responses for waveguides have been derived around a modal basis. Thus the theory offers a complimentary approach to ray theory estimates of waveguide impulse responses.

The theory presented here is useful for estimating the upper bound of time series stability or predictability for waveguides which experience random fluctuations. The theory requires these fluctuations to be characterized by some number of uncorrelated empirical orthogonal functions, each with its own power and horizontal correlation length scale. The theory estimates the degree to which these sound speed fluctuations affect the phase of the individual modes, and the time of flight of the mode packets to the receiver. The more EOFs are used to describe the water column variability, the more the acoustic modes become uncorrelated from one another. As the modes become uncorrelated, their coherent sum becomes less predictable, and consequently the ensemble average of the time series becomes smoother and lower in amplitude than any particular perturbed or unperturbed realization. Thus the theory predicts the "defocusing" of the arrival structure in the time-depth plane which occurs over many independent realizations. In practice, this defocusing can be expected to occur over time scales of the ocean process which introduces the sound speed fluctuations.

The theory estimates the upper bound of the time series predictability because it relies on the least harsh model for propagation through water column variability; the adiabatic approximation. While the mode shapes and the wavenumbers are acknowledged to be strong functions of frequency in the underlying propagation theory, the sound speed perturbations are assumed to affect only the travel time and the accumulated phase of the individual modes. Thus mode coupling, the exchange of energy into and out of modes caused by abrupt transitions of sound speed or even by long accumulations of small coupling effects, is ignored. Even more prosaic effects such as the change in the mode shapes due to the sound speed perturbations are neglected. These assumptions imply that the theory takes a view of the effects of water column variability on modal propagation which is almost benign.

The simplifying assumptions make possible the derivation of closed form expressions

for the ensemble average of the STA of the intensity received in a waveguide. For the first time, these types of expressions are now available for evaluating time series stability as a function of the modal characteristics of the waveguide at the center frequency and the spatial characteristics of the sound speed perturbations in the waveguide. The requirements for running Monte-Carlo simulations are removed, and Fourier synthesis is no longer required, so that a lower bound analysis of the magnitude of the variability effects can be quickly obtained in closed form with the insight that affords.

The theory was used to estimate the effects of internal wave activity on the predictability of time series in shallow water and in a SOFAR channel. The results showed that for realistic sound speed perturbations caused by a Garrett-Munk spectrum with an amplitude of 320 m^2cph, the lowest order modes in both propagation scenarios had the most unpredictable phases and arrival times. In the shallow water profile the result was that the onset of the arrival structure, associated with the lowest order modes, became less predictable, while the later arrivals associated with the higher order modes and bearing a strong relation to bottom-surface multiples were quite stable. In the SOFAR channel the crescendo on the channel axis, again associated with the lower order modes, was the least predictable component of the time series, while the higher angle precursors, while somewhat unpredictable in travel time, none the less proved themselves to be relatively insensitive to the sound speed perturbations introduced by 1 GM.

Finally, the theory was utilized in its first application, to estimate in closed form the expected value of the defocusing in the ensemble sense of a time reversal mirror. The results shown for the shallow water case indicated that 1 GM could introduce substantial defocusing in time and depth even while the time series themselves appeared to be quite predictable and stable. For SOFAR propagation, the performance degradation was less severe, but both results indicated that once the correlation time scale of the water column is exceeded, significant blurring about the focus depth, and by extension focus range, can be expected to occur. While this was known before, a lower bound on the defocusing may now be quickly and easily obtained. Since the results are given in closed form, it is hoped that a better understanding of the defocusing phenomena may be formed.

References

[1] J. F Lynch, G. Jin, R. Pawlowicz, D. Ray, A. J. Plueddemann, C-S. Chiu, J. H. Miller, R. H. Bourke, A. R. Parsons and R. Muench, "Acoustic travel-time perturbations due to shallow-water internal waves and internal tides in the Barents Sea Polar Front: Theory and experiment," J. Acoust. Soc. Am., **99** (2) 803-821 (1996)

[2] P. Traykovski, "Travel-time perturbations due to internal waves: Equivalence of modal and ray solutions," J. Acoust. Soc. Am., **99** (2) 822-830 (1996)

[3] J. L. Krolik, "Matched field minimum variance beamforming in a random ocean channel," J. Acoust. Soc. Am., **92** (3) 1408-1419 (1992)

[4] K. D. LePage, *Covariance of incident field in a shallow water waveguide: coherence with rough surface scattering and formal average*, BBN memorandum, May 9, 1997

[5] D. R. Jackson and D. R. Dowling, "Phase conjugation in underwater acoustics," J. Acoust. Soc. Am., **89** (3) 171-181 (1991)

[6] M Fink, "Time Reversed Acoustics," Phys. Today **50**, 34-40 (March 1997)

[7] W. S. Hodgkiss, H. C. Song, W. A. Kuperman, T. Akal, C. Ferla and D. R. Jackson, "A long-range and variable focus phase-conjugation experiment in shallow water," J. Acoust. Soc. Am., **105** (3) 1597-1604 (1999)

[8] *PROSIM (PROpagation channel SIMulator). First year technical report,* TMS SAS 97/S/EGS/NC/084 AP (1998)

[9] A. J. Elliot and J. F. E. Jackson, "Internal waves and acoustic variability," *Proc. of the IEEE Oceans'98 Conference* (1998).

[10] P. L. Nielsen, F. Bini-Verona and F. B. Jensen, "Environmental and acoustic data collected south of the island of Elba during the PROSIM'97 experiment," SACLANT Undersea Research Centre SM-357, La Spezia, Italy (1999).

[11] W. H. Munk, "Sound channel in an exponentially stratified ocean with applications to SOFAR," J. Acoust. Soc. Am., **55**, 220-226 (1974)

[12] J. A. Colosi, S. M. Flatte and C. Bracher, "Internal-wave effects on 1000-km oceanic acoustic pulse propagation: Simulation and comparison with experiment," J. Acoust. Soc. Am., **96** (1) 452-468 (1994)

[13] J. A. Colosi and S. M. Flatte, "Mode coupling by internal waves for multi-megameter acoustic propagation in the ocean," J. Acoust. Soc. Am., **100** (6) 3607-3620 (1996)

Annex A
Evaluation of frequency integrals for $\langle p^2_{STA} \rangle$

We wish to evaluate the following frequency integrals

$$\begin{aligned}\rho^2_{nm,r,t}(\omega_o, \triangle\omega) &= e^{-\Theta^2_{nm}} \int_{-\infty}^{\infty} d\omega_1 \, e^{-\omega_1(\Theta^2_1 + i\tau_n)} e^{-\omega_1^2(\Theta^2_{11} + 1/2\triangle\omega^2)} \\ &\quad \times \int_{-\infty}^{\infty} d\omega_2 \, \exp(-\omega_2(\underbrace{\Theta^2_2 - i\tau_m - \omega_1\Theta^2_{12}}_{B_2})) \\ &\quad \cdot \exp(-\omega_2^2(\underbrace{\Theta^2_{22} + 1/2\,\triangle\omega^2}_{A_2})), \end{aligned} \tag{27}$$

where $\tau_{n,m} = t - \int_0^\tau S_{n,m}(r')\,dr'$ for compactness of notation. Completing the square, the ω_2 integral may be evaluated, reducing Eq. (27) to

$$\begin{aligned}\rho^2_{nm,r,t}(\omega_o, \triangle\omega) &= \sqrt{\pi/A_2} e^{(\Theta^2_2 - i\tau_m)^2/4A_2} e^{-\Theta^2_{nm}} \\ &\quad \times \int_{-\infty}^{\infty} d\omega_1 \, \exp(-\omega_1(\underbrace{\Theta^2_1 + i\tau_n - (2i\Theta^2_{12}\tau_m - 2\Theta^2_2\Theta^2_{12})/4A_2}_{B_1})) \\ &\quad \cdot \exp(-\omega_1^2(\underbrace{\Theta^2_{11} + 1/2\,\triangle\omega^2 - \Theta^4_{12}/4A_2}_{A_1})). \end{aligned} \tag{28}$$

Completion of the square to the argument of the exponential inside the integral over ω_1 and evaluation of the integral yields

$$\begin{aligned}\rho^2_{nm,r,t}(\omega_o, \triangle\omega) &= \sqrt{\pi/A_1}\sqrt{\pi/A_2} e^{-\Theta^2_{nm}} \\ &\quad \cdot \; e^{B_1^2/4A_1} e^{(\Theta^2_2 - i\tau_m)^2/4A_2}, \end{aligned} \tag{29}$$

which upon explicit evaluation of the parameters A_1, B_1 and A_2 yields Eq. (12) as desired.

Annex B

Evaluation of frequency integrals for σ^2_{STA}

Upon squaring out the argument to the probability term on the fifth line of Eq. (13), we find it useful to define the following constants for the evaluation of the frequency integrals over ω_1, ω_2, $\omega_{1'}$ and $\omega_{2'}$

$$
\begin{aligned}
\Theta^2_{nmn'm'} &= \sum_e (\triangle k_{en} + \triangle k_{en'} - \triangle k_{em} - \triangle k_{em'}) \sigma^2_{g_e} r\ell_e/2 \\
\Theta^2_1 &= \sum_e (\triangle k_{en} + \triangle k_{en'} - \triangle k_{em} - \triangle k_{em'}) \triangle S_{en} \sigma^2_{g_e} r\ell_e) \\
\Theta^2_2 &= -\sum_e (\triangle k_{en} + \triangle k_{en'} - \triangle k_{em} - \triangle k_{em'}) \triangle S_{em} \sigma^2_{g_e} r\ell_e \\
\Theta^2_{1'} &= \sum_e (\triangle k_{en} + \triangle k_{en'} - \triangle k_{em} - \triangle k_{em'}) \triangle S_{en'} \sigma^2_{g_e} r\ell_e) \\
\Theta^2_{2'} &= -\sum_e (\triangle k_{en} + \triangle k_{en'} - \triangle k_{em} - \triangle k_{em'}) \triangle S_{em'} \sigma^2_{g_e} r\ell_e \\
\Theta^2_{11} &= \sum_e \triangle S^2_{en} \sigma^2_{g_e} r\ell_e/2 + 1/2 \triangle \omega^2 \\
\Theta^2_{12} &= \sum_e \triangle S_{en} \triangle S_{em} \sigma^2_{g_e} r\ell_e \\
\Theta^2_{11'} &= \sum_e \triangle S_{en} \triangle S_{en'} \sigma^2_{g_e} r\ell_e \\
\Theta^2_{12'} &= \sum_e \triangle S_{en} \triangle S_{em'} \sigma^2_{g_e} r\ell_e \\
\Theta^2_{22} &= \sum_e \triangle S^2_{em} \sigma^2_{g_e} r\ell_e/2 + 1/2 \triangle \omega^2 \\
\Theta^2_{21'} &= \sum_e \triangle S_{em} \triangle S_{en'} \sigma^2_{g_e} r\ell_e \\
\Theta^2_{22'} &= \sum_e \triangle S_{em} \triangle S_{em'} \sigma^2_{g_e} r\ell_e \\
\Theta^2_{1'1'} &= \sum_e \triangle S^2_{en'} \sigma^2_{g_e} r\ell_e/2 + 1/2 \triangle \omega^2 \\
\Theta^2_{1'2'} &= \sum_e \triangle S_{en'} \triangle S_{em'} \sigma^2_{g_e} r\ell_e \\
\Theta^2_{2'2'} &= \sum_e \triangle S^2_{em'} \sigma^2_{g_e} r\ell_e/2 + 1/2 \triangle \omega^2.
\end{aligned}
$$

Using these constants, the frequency integrals may be rewritten in the condensed

format

$$\begin{aligned}
\rho_{nmn'm'} &= e^{-\Theta^2_{nmn'm'}} \int_{-\infty}^{\infty} d\omega_1\ e^{-\omega_1(\Theta_1^2 + i\tau_n(r))} e^{-\omega_1^2\Theta_{11}^2} \\
&\quad \times \int_{-\infty}^{\infty} d\omega_2\ e^{-\omega_2(\Theta_2^2 - \omega_1\Theta_{12}^2 - i\tau_m(r))} e^{-\omega_2^2\Theta_{22}^2} \\
&\quad \times \int_{-\infty}^{\infty} d\omega_{1'}\ e^{-\omega_{1'}(\Theta_{1'}^2 - \omega_2\Theta_{1'2}^2 + \omega_1\Theta_{1'1}^2 + i\tau_{n'}(r))} e^{-\omega_{1'}^2\Theta_{1'1'}^2} \\
&\quad \times \int_{-\infty}^{\infty} d\omega_{2'}\ \exp(-\omega_{2'} \underbrace{(\Theta_{2'}^2 - \omega_{1'}\Theta_{2'1'}^2 + \omega_2\Theta_{2'2}^2 - \omega_1\Theta_{2'1}^2 - i\tau_{m'}(r))}_{B_{2'}}) \\
&\quad \cdot \exp(-\omega_{2'}^2 \underbrace{\Theta_{2'2'}^2}_{A_{2'}}), \qquad (30)
\end{aligned}$$

where henceforth $\tau_{n,m} \equiv (t - \tau_{n,m}(r))$. Integration over $\omega_{2'}$ yields a term of the form

$$\sqrt{\pi/A_{2'}} \exp(B_{2'}^2/4A_{2'}).$$

Squaring out $B_{2'}$ and separating out terms which are independent of ω_1, ω_2 and $\omega_{1'}$, Eq. (30) may be written

$$\begin{aligned}
\rho_{nmn'm'} &= \sqrt{\pi/A_{2'}} \exp(C_{2'}^2/4A_{2'}) e^{-\Theta^2_{nmn'm'}} \\
&\quad \times \int_{-\infty}^{\infty} d\omega_1\ \exp(-\omega_1(\Theta_1^2 + i\tau_n(r) + \underbrace{\Theta_{2'1}^2 2(\Theta_{2'}^2 - i\tau_{m'})/4\Theta_{2'2'}^2}_{C_{12'}})) \\
&\quad \cdot \exp(-\omega_1^2(\Theta_{11}^2 \underbrace{-\Theta_{2'1}^4/4\Theta_{2'2'}^2}_{C_{12'}^2})) \\
&\quad \times \int_{-\infty}^{\infty} d\omega_2\ \exp(-\omega_2(\Theta_2^2 - i\tau_m(r) \underbrace{-2\Theta_{2'2}^2(\Theta_{2'}^2 - i\tau_{m'})/4\Theta_{2'2'}^2}_{C_{22'}})) \\
&\quad \cdot \exp(\omega_2(\omega_1(\underbrace{\Theta_{12}^2 - 2\Theta_{2'2}^2\Theta_{2'1}^2/4\Theta_{2'2'}^2}_{C_{21}}))) \\
&\quad \cdot \exp(-\omega_2^2(\Theta_{22}^2 \underbrace{-\Theta_{2'2}^4/4\Theta_{2'2'}^2}_{C_{2'2}^2})) \\
&\quad \times \int_{-\infty}^{\infty} d\omega_{1'}\ \exp(-\omega_{1'}(\underbrace{\Theta_{1'}^2 + i\tau_{n'}(r) + 2\Theta_{2'1'}^2(\Theta_{2'}^2 - i\tau_{m'})/4\Theta_{2'2}^2}_{C_{1'}})) \\
&\quad \cdot \exp(\omega_{1'}(\omega_2(\underbrace{\Theta_{1'2}^2 - 2\Theta_{2'1'}^2\Theta_{2'2}^2/4\Theta_{2'2'}^2}_{C_{21'}}))) \\
&\quad \cdot \exp(-\omega_{1'}(\omega_1(\underbrace{\Theta_{1'1}^2 - 2\Theta_{2'1'}^2\Theta_{2'1}^2/4\Theta_{2'2'}^2}_{C_{11'}}))) \\
&\quad \cdot \exp(-\omega_{1'}^2(\underbrace{\Theta_{1'1'}^2 - \Theta_{2'1'}^4/4/\Theta_{2'2'}^2}_{A_{1'}})), \qquad (31)
\end{aligned}$$

where

$$C_{2'} = \Theta_{2'}^2 - i\tau_{m'}.$$

Completing the square of the argument to the exponential kernel in the $\omega_{1'}$ integral, we obtain

$$\begin{aligned}
\rho_{nmn'm'} &= \sqrt{\pi/A_{1'}}\sqrt{\pi/A_{2'}}\exp(C_{1'}^2/4A_{1'})\exp(C_{2'}^2/4A_{2'})e^{-\Theta_{nmn'm'}^2} \\
&\quad \times \int_{-\infty}^{\infty} d\omega_1 \ \exp(-\omega_1(\Theta_1^2 + i\tau_n(r) + C_{12'} - 2C_{11'}C_{1'}/4A_{1'})) \\
&\quad \cdot \ \exp(-\omega_1^2(\Theta_{11}^2 + C_{12'}^2 - C_{11'}^2/4A_{1'})) \\
&\quad \times \int_{-\infty}^{\infty} d\omega_2 \ \exp\left(-\omega_2\left(\underbrace{\begin{array}{c}\Theta_2^2 - i\tau_m(r) + C_{22'} + 2C_{21'}C_{1'}/4A_{1'} \\ +\omega_1(2C_{21'}C_{11'}/4A_{1'} - C_{21})\end{array}}_{B_2}\right)\right) \\
&\quad \cdot \ \exp(-\omega_2^2(\underbrace{\Theta_{22}^2 + C_{2'2}^2 - C_{21'}^2/4A_{1'}}_{A_2})) \qquad (32)
\end{aligned}$$

If we define

$$C_2 = \Theta_2^2 - i\tau_m + C_{22'} + 2C_{21'}C_{1'}/4A_{1'}$$

and

$$C_{12} = 2C_{21'}C_{11'}/4A_{1'} - C_{21},$$

then the ω_2 integral yields

$$\sqrt{\pi/A_2}\exp((C_2^2 + \omega_1 2C_2C_{12} + \omega_1^2 C_{12}^2)/4A_2).$$

Then Eq. (32) may be written

$$\begin{aligned}
\rho &= \sqrt{\pi/A_2}\sqrt{\pi/A_{1'}}\sqrt{\pi/A_{2'}}\exp(C_2^2/4A_2)\exp(C_{1'}^2/4A_{1'})\exp(C_{2'}^2/4A_{2'})e^{-\Theta_{nmn'm'}^2} \\
&\quad \times \int_{-\infty}^{\infty} d\omega_1 \ \exp(-\omega_1(\underbrace{\Theta_1^2 + i\tau_n(r) + C_{12'} - 2C_{11'}C_{1'}/4A_{1'} - 2C_{12}C_2/4A_2}_{B_1})) \\
&\quad \cdot \ \exp(-\omega_1^2(\underbrace{\Theta_{11}^2 + C_{12'}^2 - C_{11'}^2/4A_{1'} - C_{12}^2/4A_2}_{A_1})). \qquad (33)
\end{aligned}$$

Evaluation of the ω_1 integral yields the desired solution

$$\begin{aligned}
\rho_{nmn'm'} &= \sqrt{\pi/A_1}\sqrt{\pi/A_2}\sqrt{\pi/A_{1'}}\sqrt{\pi/A_{2'}}e^{-\Theta_{nmn'm'}^2} \\
&\quad \times \exp(C_1^2/4A_1)\exp(C_2^2/4A_2)\exp(C_{1'}^2/4A_{1'})\exp(C_{2'}^2/4A_{2'}), \qquad (34)
\end{aligned}$$

where

$$C_1 = B_1^2/4A_1.$$

Annex C

Evaluation of frequency integrals for Type 2 correction to expressions for $\langle p_{STA}^2 \rangle$

For p_{STA}^2 for Type 2 narrow band approximation, we wish to evaluate the follow integrals (assuming for the moment that a single mode function is a function of frequency, this simplifies the expressions but does not affect the final answer as the necessary cross terms in terms of the expressions derived here can easily be determined")

$$\int d\omega_1 \left(\phi_n + \omega_1 \frac{\partial \phi_n}{\partial \omega}\right) e^{-\omega_1(\Theta_1^2 + i\tau_n)} e^{-\omega_1^2(\Theta_{11}^2 + T^2)}$$
$$\times \int d\omega_2 \left(\phi_m + \omega_2 \frac{\partial \phi_m}{\partial \omega}\right) \exp(-\omega_2 \underbrace{(\Theta_2^2 - i\tau_m - \omega_1 \Theta_{12}^2)}_{B_2}) \exp(-\omega_2^2 \underbrace{(\Theta_{22}^2 + T^2)}_{A_2}).$$

But

$$\int d\omega_2 \, \omega_2 \frac{\partial \phi_m}{\partial \omega} e^{-\omega_2^2 A_2} e^{-\omega_2 B_2} = -\sqrt{\phi/A_2} e^{B_2^2/4A_2} \frac{B_2}{2A_2} \frac{\partial \phi_m}{\partial \omega},$$

so what remains to be evaluated is the integral

$$\int d\omega_1 \left(\phi_n + \omega_1 \frac{\partial \phi_n}{\partial \omega}\right) e^{-\omega_1(\Theta_1^2 + i\tau_n)} e^{-\omega_1^2(\Theta_{11}^2 + T^2)}$$
$$\times \sqrt{\phi/A_2} e^{B_2^2(\omega_1)/4A_2} \left(\phi_m - \frac{B_2(\omega_1)}{2A_2} \frac{\partial \phi_m}{\partial \omega}\right), \tag{35}$$

which may be written

$$\int d\omega_1 \left(\phi_n + \omega_1 \frac{\partial \phi_n}{\partial \omega}\right) e^{-\omega_1(\Theta_1^2 + i\tau_n)} e^{-\omega_1^2(\Theta_{11}^2 + T^2)}$$
$$\times \sqrt{\phi/A_2} e^{B_2^2(\omega_1)/4A_2} \left(\phi_m - \left(\frac{B_2'(\omega_1)}{2A_2} - \frac{\omega_1 \Theta_{12}^2}{2A_2}\right) \frac{\partial \phi_m}{\partial \omega}\right), \tag{36}$$

which may be written as four integrals, the first of which is a normal Gaussian integral, the second and third have the form of a first moment, and the third the form of a second moment

$$\sqrt{\pi/A_2} \left\{ \int d\omega_1 \left(\phi_n \left(\phi_m - \frac{B_2'}{2A_2} \frac{\partial \phi_m}{\partial \omega}\right)\right) e^{-\omega_1(\Theta_1^2 + i\tau_n)} e^{-\omega_1^2(\Theta_{11}^2 - T^2)} e^{B_2^2/4A_2} \right.$$
$$\left. + \int d\omega_1 \left(\phi_n \frac{\partial \phi_m}{\partial \omega} \frac{\Theta_{12}^2}{2A_2}\right) \omega_1 \, e^{-\omega_1(\Theta_1^2 + i\tau_n)} e^{-\omega_1^2(\Theta_{11}^2 - T^2)} e^{B_2^2/4A_2} \right.$$

$$+ \int d\omega_1 \left(\phi_m - \frac{B_2'}{2A_2}\frac{\partial\phi_m}{\partial\omega}\right)\frac{\partial\phi_n}{\partial\omega}\,\omega_1\, e^{-\omega_1(\Theta_1^2+i\tau_n)}e^{-\omega_1^2(\Theta_{11}^2-T^2)}e^{B_2^2/4A_2}$$
$$+ \int d\omega_1 \left(\frac{\partial\phi_n}{\partial\omega}\frac{\partial\phi_m}{\partial\omega}\frac{\Theta_{12}^2}{2A_2}\right)\omega_1^2\, e^{-\omega_1(\Theta_1^2+i\tau_n)}e^{-\omega_1^2(\Theta_{11}^2-T^2)}e^{B_2^2/4A_2}\Bigg\}. \qquad (37)$$

Eq. (38) may be rewritten

$$\sqrt{\pi/A_2}\Bigg\{\int d\omega_1 \left(\phi_n\left(\phi_m - \frac{B_2'}{2A_2}\frac{\partial\phi_m}{\partial\omega}\right)\right)e^{-\omega_1 B_1}e^{-\omega_1^2 A_1}e^{B_2^2/4A_2}$$
$$+ \int d\omega_1 \Bigg(\underbrace{\phi_n\frac{\partial\phi_m}{\partial\omega}\frac{\Theta_{12}^2}{2A_2} + \left(\phi_m - \frac{B_2'}{2A_2}\frac{\partial\phi_m}{\partial\omega}\right)\frac{\partial\phi_n}{\partial\omega}}_{\mathbf{A}}\Bigg)\,\omega_1\, e^{-\omega_1 B_1}e^{-\omega_1^2 A_1}e^{B_2^2/4A_2}$$
$$+ \int d\omega_1 \Bigg(\underbrace{\frac{\partial\phi_n}{\partial\omega}\frac{\partial\phi_m}{\partial\omega}\frac{\Theta_{12}^2}{2A_2}}_{\mathbf{B}}\Bigg)\omega_1^2\, e^{-\omega_1 B_1}e^{-\omega_1^2 A_1}e^{B_2^2/4A_2}\Bigg\}e^{(\Theta_2^2-i\tau_m)^2/2A_2}, \qquad (38)$$

which equals

$$\sqrt{\pi/A_2}\sqrt{\pi/A_1}e^{B_1^2/4A_1}e^{(\Theta_2^2-i\tau_m)^2/4A_2}$$
$$+ \sqrt{\pi/A_2}e^{(\Theta_2^2-i\tau_m)^2/4A_2}\mathbf{A}\int d\omega_1\,\omega_1\, e^{-\left(\omega_1 A_1^{1/2}+B_1/2A_1^{1/2}\right)^2}e^{B_1^2/4A_1}$$
$$+ \sqrt{\pi/A_2}e^{(\Theta_2^2-i\tau_m)^2/4A_2}\mathbf{B}\int d\omega_1\,\omega_1^2\, e^{-\left(\omega_1 A_1^{1/2}+B_1/2A_1^{1/2}\right)^2}e^{B_1^2/4A_1}, \qquad (39)$$

where B_1 and A_1 are defined in the Annex A.

We know that

$$\int d\omega \left(\omega_1 + \frac{B_1}{2A_1}\right)e^{-\left(\omega_1 A_1^{1/2}+B_1/2A_1^{1/2}\right)^2}e^{B_1^2/4A_1} \equiv 0,$$

so the second line of Eq. (39) equals

$$-\mathbf{A}\frac{B_1}{2A_1}\sqrt{\pi/A_1}\sqrt{\pi/A_2}\; e^{(\Theta_2^2-i\tau_m)^2/4A_2}\; e^{B_1^2/4A_1}.$$

For the second moment we know that

$$\int d\omega \left(\omega_1 + \frac{B_1}{2A_1}\right)^2 e^{-\left(\omega_1 A_1^{1/2}+B_1/2A_1^{1/2}\right)^2}e^{B_1^2/4A_1} \equiv \sqrt{\pi},$$

so the third line of Eq. (39) equals

$$\mathbf{B}\left(\frac{1}{2A_1}+\frac{B_1^2}{4A_1}\right)\sqrt{\pi/A_1}\sqrt{\pi/A_2}e^{(\Theta_2^2-i\tau_m)^2/4A_2}\ e^{B_1^2/4A_1}.$$

Thus the expression for p_{STA}^2 has as its kernel the expression

$$\begin{aligned}
&\sqrt{\pi/A_2}\sqrt{\pi/A_1}e^{B_1^2/4A_1}e^{(\Theta_2^2-i\tau_m)^2/4A_2}\\
&\quad\times\ \left\{\phi_n\left(\phi_m-\frac{B_2'}{2A_2}\frac{\partial\phi_m}{\partial\omega}\right)\right.\\
&\qquad-\left(\phi_n\frac{\partial\phi_m}{\partial\omega}\frac{\Theta_{12}^2}{2A_2}+\left(\phi_m-\frac{B_2'}{2A_2}\frac{\partial\phi_m}{\partial\omega}\right)\frac{\partial\phi_n}{\partial\omega}\right)\frac{B_1}{2A_1}\\
&\qquad\left.+\left(\frac{\partial\phi_n}{\partial\omega}\frac{\partial\phi_m}{\partial\omega}\frac{\Theta_{12}^2}{2A_2}\right)\left(\frac{1}{2A_1}+\frac{B_1^2}{4A_1}\right)\right\}
\end{aligned}\tag{40}$$

Document Data Sheet

NATO UNCLASSIFIED

Security Classification		Project No.
UNCLASSIFIED		04-D
Document Serial No.	**Date of Issue**	**Total Pages**
SR-319	July 1999	49 pp.

Author(s)

LePage, K.D.

Title

Time series variability in fluctuating ocean waveguides.

Abstract

The variability of signals propagating through an uncertain sound speed structure is addressed. Signals are assumed to travel in a narrow band adiabatically in modes and to experience fluctuations in sound speed which are characterized according to the vertical and horizontal distributions of these fluctuations. The sound speed fluctuations are assumed to affect only the phases speed and the group speed of the modes in a perturbative way. The changes in the local phase and group speeds are expanded for small perturbations to the sound speed. Sound speed perturbations are described in terms of their statistical characteristics. Vertically, the sound speed fluctuations are decomposed into empirical orthogonal functions (EOFs), while horizontally they are assumed to be correlated on some horizontal length scale much smaller than the propagation ranges of interest. Thus the cumulative phase and group speed fluctuations over the propagation path are assumed to be distributed Gaussian according to the central limit theorem.

The framework outlined above is used to derive the first and second moments of the signal envelope received over an ensemble of ocean realizations following the distribution properties outlined above. Since the mean and variance of the expected signal are obtained in the time domain, the stability of model arrivals in time can be predicted for a variety of different sound speed fluctuation distributions. Since the phase and group speed fluctuations are linear in identical terms involving the inner product of the mode shape functions with the EOFs, the fluctuations of these quantities are entirely correlated. However, as the different EOFs express themselves differently on each set of propagating modes, the model interference structure becomes less certain due to the fluctuations. The theory estimates this degree of decorrelation as a function of the signal, waveguide and fluctuation parameters.

In order to benchmark the theory, the first moment of the short time average of the signal intensity is also predicted using realizations of propagation through an ensemble of sound speed fluctuations consistent with the statistical description. Excellent agreement is found between these self-consistent Monte-Carlo estimates of the signal variability and the closed form expressions.

Keywords

Signal fluctuations - empirical orthogonal functions (EOF) - complex envelope - narrowband - time reversal mirror - internal waves

Issuing Organization

North Atlantic Treaty Organization
SACLANT Undersea Research Centre
Viale San Bartolomeo 400, 19138 La Spezia, Italy

[From N. America: SACLANTCEN (New York) APO AE 09613]

Tel: +39 0187 527 361
Fax:+39 0187 524 600

E-mail: library@saclantc.nato.int

NATO UNCLASSIFIED

Initial Distribution for SR-319

Ministries of Defence

DND Canada	10
CHOD Denmark	8
MOD Germany	15
HNDGS Greece	12
MARISTAT Italy	9
MOD (Navy) Netherlands	12
NDRE Norway	10
MOD Portugal	5
MDN Spain	2
TDKK and DNHO Turkey	5
MOD UK	20
ONR USA	32

NATO Commands and Agencies

NAMILCOM	2
SACLANT	3
CINCEASTLANT/ COMNAVNORTHWEST	1
CINCIBERLANT	1
CINCWESTLANT	1
COMASWSTRIKFOR	1
COMSTRIKFLTANT	1
COMSUBACLANT	1
SACLANTREPEUR	1
SACEUR	2
CINCNORTHWEST	1
CINCSOUTH	1
COMEDCENT	1
COMMARAIRMED	1
COMNAVSOUTH	1
COMSTRIKFORSOUTH	1
COMSUBMED	1
NC3A	1
PAT	1

Scientific Committee of National Representatives

SCNR Belgium	1
SCNR Canada	1
SCNR Denmark	1
SCNR Germany	1
SCNR Greece	1
SCNR Italy	1
SCNR Netherlands	2
SCNR Norway	1
SCNR Portugal	1
SCNR Spain	1
SCNR Turkey	1
SCNR UK	1
SCNR USA	2
SECGEN Rep. SCNR	1
NAMILCOM Rep. SCNR	1

National Liaison Officers

NLO Canada	1
NLO Denmark	1
NLO Germany	1
NLO Italy	1
NLO Netherlands	1
NLO Spain	1
NLO UK	1
NLO USA	1

Sub-total	188
SACLANTCEN	30
Total	218